

Comparative Shear Testing and Finite Element Analysis of PowerSeal Saddle for Service Line Installations

Tianyu Han, Qinglai Zhang, Shakhzod M. Takhirov, Kenichi Soga
Center for Smart Infrastructure (CSI)
Department of Civil and Environmental Engineering
University of California, Berkeley

Prepared for PowerSeal Pipeline Products Corporation



Berkeley
CENTER FOR
Smart Infrastructure

CSI Report 2022/01
Center for Smart Infrastructure (CSI)
Department of Civil and Environmental Engineering
University of California, Berkeley
Dec 2022

EXECUTIVE SUMMARY

This report discusses the results of the experimental program focused on the performance of service saddles under monotonic shear loading. The saddles are commonly used for providing a connection between a customer service line and a larger diameter distribution pipeline for potable water. In this experimental program, the service saddles manufactured by PowerSeal Pipeline Products Corporation were compared to those currently used by the East Bay Municipal Utility District (EBMUD). The tests were conducted under shear loading up to failure of the saddle or a significant leak. The performance of the finite element model was validated using the experimental results obtained from distributed fiber optic sensors, which can be used to examine and predict the behavior of the pipe and saddle in whole process. The knowledge gained from the comprehensive laboratory tests and finite element models provides the reference for future test improvements and optimization in the saddle design.

Keywords: *Saddle, service line, water pipelines, leakage, finite element analysis*

ACKNOWLEDGMENTS

The funding for this project was provided by PowerSeal Pipeline Products Corporation, which is greatly appreciated. The successful completion of the work would not be possible without the strong support of the lab personnel. Special thanks are due to Llyr Griffith, John Kochan, Phillip Wong of the University of California, Berkeley (UC Berkeley) for their work on the experimental setup and conducting the tests. An active involvement of and a guidance from Yuuki Tanaka and David Katzev of EBMUD is greatly appreciated. The project's research team also included a number of students focused on fiber-optic sensing. Special thanks are due to Shih-Hung Chiu and Chien-Chih Wang of UC Berkeley for their work on these tasks.

DISCLAIMER

Any opinions, findings, and conclusions or recommendations expressed in this material are those of the author(s) and do not necessarily reflect those of the University of California, Berkeley.

CONTENTS

EXECUTIVE SUMMARY	II
ACKNOWLEDGMENTS	III
DISCLAIMER.....	IV
CONTENTS.....	V
LIST OF FIGURES	VII
LIST OF TABLES	IX
1 INTRODUCTION.....	1
2 EXPERIMENTAL SETUP	1
3 INSTRUMENTATION AND SPECIMEN LIST	4
3.1 Locations of Conventional Instruments	5
3.2 Location of Fiber-optic Sensors.....	6
3.3 Test Specimens	7
4 TEST RESULTS OF CONVENTIONAL INSTRUMENTS	8
4.1 Test Data Analysis	9
4.2 Failure Modes	11
4.3 Comparative Summary of Test Data.....	12
5 TEST RESULTS OF FIBER-OPTIC SENSORS	14
5.1 Test Data Analysis	15
5.1.1 Comparison between strain gage and fiber-optic data	18
5.1.2 Comparison between benchmark and PowerSeal saddles	20
5.1.3 Comparison of PowerSeal saddles with different torques	23
5.1.4 Comparison of PowerSeal saddles with different straps.....	26
6 FINITE ELEMENT ANALYSIS.....	29
6.1 Overview of Numerical Model	29

6.2	Determination of Rubber Interface	30
6.3	Determination of Material Parameters	31
6.4	FEM Results & Discussions	31
6.4.1	Overview of FE analysis	31
6.4.2	Comparison of the FEM results and experimental fiber-optic data	32
7	CONCLUSIONS	36
8	REFERENCES.....	37
APPENDIX A:	SPECIFICATIONS OF POWERSEAL SADDLE	38
APPENDIX B:	PHOTOS OF TESTED SPECIMENS	41
APPENDIX C:	DISTRIBUTED FIBER OPTIC SENSING.....	46
APPENDIX D:	TEST RESULTS OF FIBER-OPTIC SENSORS	48
APPENDIX E:	FINITE ELEMENT RESULTS.....	61

LIST OF FIGURES

Figure 1-1. PowerSeal model 3450AS saddle	1
Figure 2-1. Schematic drawing of experimental setup	2
Figure 2-2. Drilling a tap hole in distribution pipeline through a saddle.....	3
Figure 2-3. Overall view	4
Figure 2-4. Detail of load application	4
Figure 3-1. Locations of conventional instruments	5
Figure 3-2. Additional position transducer at saddle	6
Figure 3-3. Locations of fiber-optic sensors for the Benchmark saddle.....	7
Figure 3-4. Locations of fiber-optic sensors for the PowerSeal saddle	7
Figure 3-5. Straps with lower capacity	8
Figure 4-1. Test results for 70 ft-lb torque.....	9
Figure 4-2. Test results for 85 ft-lb torque.....	10
Figure 4-3. Test results for 100 ft-lb torque.....	10
Figure 4-4. Test results for PowerSeal saddles with different straps at 85 ft-lb torque.....	11
Figure 4-5. Typical failure of benchmark saddle.....	11
Figure 4-6. PowerSeal saddle: dripping water leak close to the maximum force.....	12
Figure 4-7. Normalized displacement.....	13
Figure 4-8. Normalized force.....	14
Figure 5-1. Index for the fiber-optic cables for Benchmark1 and Benchmark3	15
Figure 5-2. Index for the fiber-optic cables for PS1	16
Figure 5-3. Index for the fiber-optic cables for PS2, PS3, and PS4	16
Figure 5-4. Location of Sensor 7 (the blue segment along the longitudinal direction of the pipeline)	17
Figure 5-5. Location of Sensor 8 (the blue segment along the circumferential direction of the pipeline)	18
Figure 5-6. Location of Sensor 13 (the blue segment on the strap)	18
Figure 5-7. Comparison between the strain gage and fiber-optic data in the longitudinal direction on the pipeline.....	19
Figure 5-8. Comparison between the strain gage and fiber-optic data in the circumferential direction on the pipeline.....	19
Figure 5-9. Locations of strain gages and the data points of fiber-optic sensors for BM1	20
Figure 5-10. Strain distribution on Sensor 7 at load of 5500 lbs.	21
Figure 5-11. Maximum strain on Sensor 7	21
Figure 5-12. Strain distribution on Sensor 8 at load of 5500 lbs.	22
Figure 5-13. Maximum and minimum strain on Sensor 8	22
Figure 5-14. Cross-section of the pipeline	23
Figure 5-15. Strain distribution on Sensor 7 at load of 9000 lbs.	23
Figure 5-16. Maximum strain on Sensor 7	24
Figure 5-17. Strain distribution on Sensor 8 at load of 9000 lbs.	24
Figure 5-18. Maximum strain on Sensor 8	24
Figure 5-19. Minimum strain on Sensor 8	25
Figure 5-20. Rotation of the saddle under pulling	25
Figure 5-21. Strain distribution on Sensor 13 at load of 9000 lbs.	26
Figure 5-22. Maximum strain on Sensor 13	26

Figure 5-23. Strain distribution on Sensor 7 at load of 9000 lbs.	27
Figure 5-24. Maximum strain on Sensor 7	27
Figure 5-25. Strain distribution on Sensor 8 at load of 9000 lbs.	28
Figure 5-26. Maximum strain on Sensor 8	28
Figure 5-27. Strain distribution on Sensor 13 at load of 9000 lbs.	29
Figure 5-28. Maximum strain on Sensor 13	29
Figure 6-1 3-D FE model mesh for saddle test	30
Figure 6-2 Coupled spring model	31
Figure 6-3 Coupled spring interaction model	32
Figure 6-4 Location of longitudinal sensors on the pipe: S1, S2, S7 (the blue segment along the longitudinal direction of the pipeline).....	32
Figure 6-5 Location of circumferential sensor on the pipe: S8 (the blue segment along the circumferential direction of the pipeline)	33
Figure 6-6 Comparison of strains on the pipe.....	34
Figure 6-7 Locations of circumferential sensors on the saddle straps: S9 and S13 (the blue segment along the circumferential direction of the pipeline)	34
Figure 6-8 (a) Comparison of strain of S13; (b) Back view of saddle setup	34
Figure 6-9 (a) Comparison of strain of S9; (b) Circumferential strain plot on strap; (c) Strain path of the FEM-middle; (d) Strain path of FEM-modify	35

LIST OF TABLES

Table 3-1. Instrumentation list	6
Table 3-2. Test log	8
Table 4-1. Summary of test results for benchmark saddle.....	12
Table 4-2. Summary of test results for PowerSeal saddle	12
Table 4-3. Summary of test results for PowerSeal saddles with different straps	14
Table 5-1. Setting for LUNA	15
Table 6-1. Material parameters	31

1 Introduction

This report discusses the results of tests conducted on a conventional saddle and the service saddle manufactured and supplied by PowerSeal Pipeline Products Corporation (PowerSeal herein). PowerSeal model 3450AS shown in Figure 1-1 was selected for this study. Specifications of the saddle are provided in Appendix A [1].



Figure 1-1. PowerSeal model 3450AS saddle

In this study, a finite element (FE) analysis is conducted to simulate the pipe and saddle behavior under monotonic shear loading. This is accomplished by utilizing an elastoplastic material model in ABAQUS and comparing the predicted values with the experimental results.

2 Experimental Setup

A special experimental setup was developed at the Center for Smart Infrastructure (CSI), UC Berkeley. It was based on the utilization of a self-reacting frame that accommodated both the loading and reacting parts as presented in Figure 2-1. Special jackets were designed and fabricated

to hold the water distribution pipeline in place. A 120-kip hydraulic actuator was used to apply the force via a loading fixture.

A ductile iron pipe manufactured by US Pipe with a nominal diameter of 6-in was used in the tests. A service tap hole in the pipe was drilled by utilizing the tools provided by EBMUD as presented in Figure 2-2. Since the service line is much more flexible than the distribution line it was assumed that their interaction is negligible. Hence, the service line was not installed.

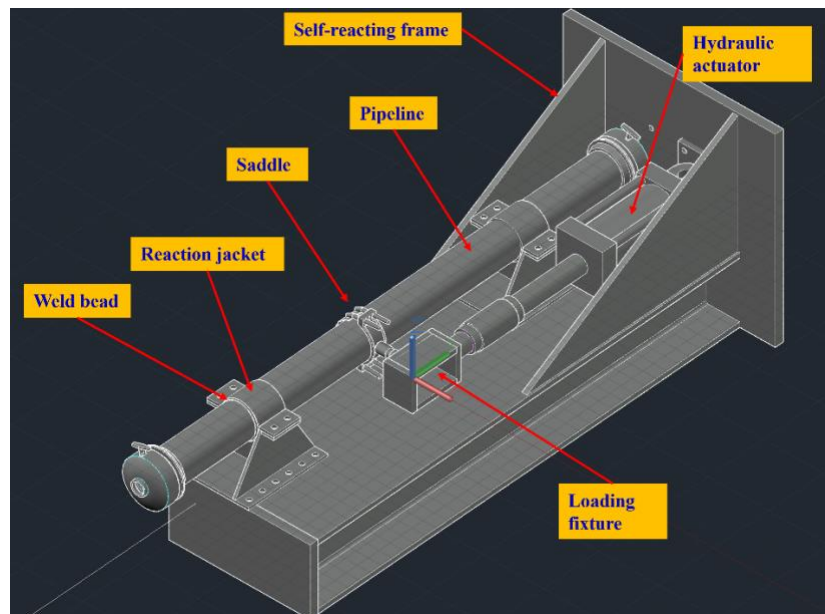


Figure 2-1. Schematic drawing of experimental setup



Figure 2-2. Drilling a tap hole in distribution pipeline through a saddle

An overall view of the fully assembled experimental setup is presented in Figure 2-3. Since the primary intention of the project was to study the saddle performance under shear loading (without applying any moment) a pivoting hoist ring was used as the loading element. This detail of the load application is presented in Figure 2-4.



Figure 2-3. Overall view

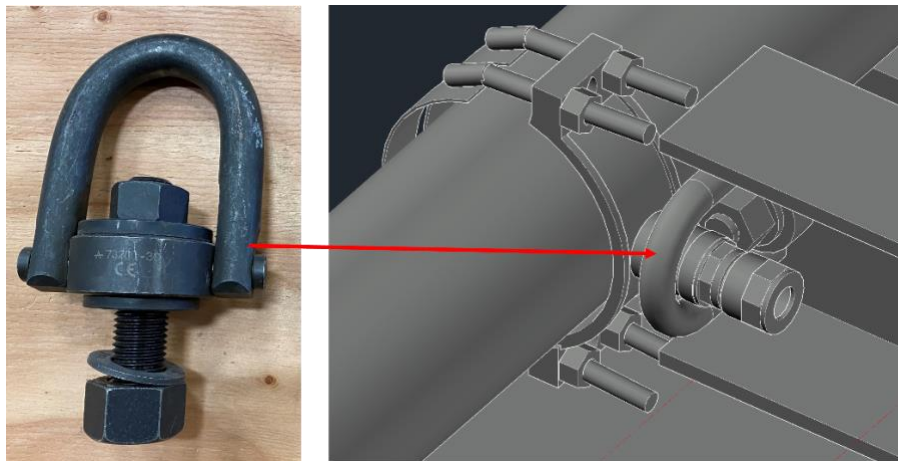


Figure 2-4. Detail of load application

3 Instrumentation and Specimen List

Instrumentation consisted of conventional instruments and fiber-optic sensors.

3.1 LOCATIONS OF CONVENTIONAL INSTRUMENTS

A schematic drawing showing the locations of the conventional instruments is presented in Figure 3-1. The actuator has a position transducer and a built-in load cell. The pipe was pressurized to 70 psi and the pressure inside of the pipe was monitored by a pressure transducer installed on one of the endcaps. An air release valve was installed on another endcap. Six strain gages were installed on the pipeline. An additional position transducer was installed to monitor the displacement of the saddle right next to the loading point as presented in Figure 3-2.

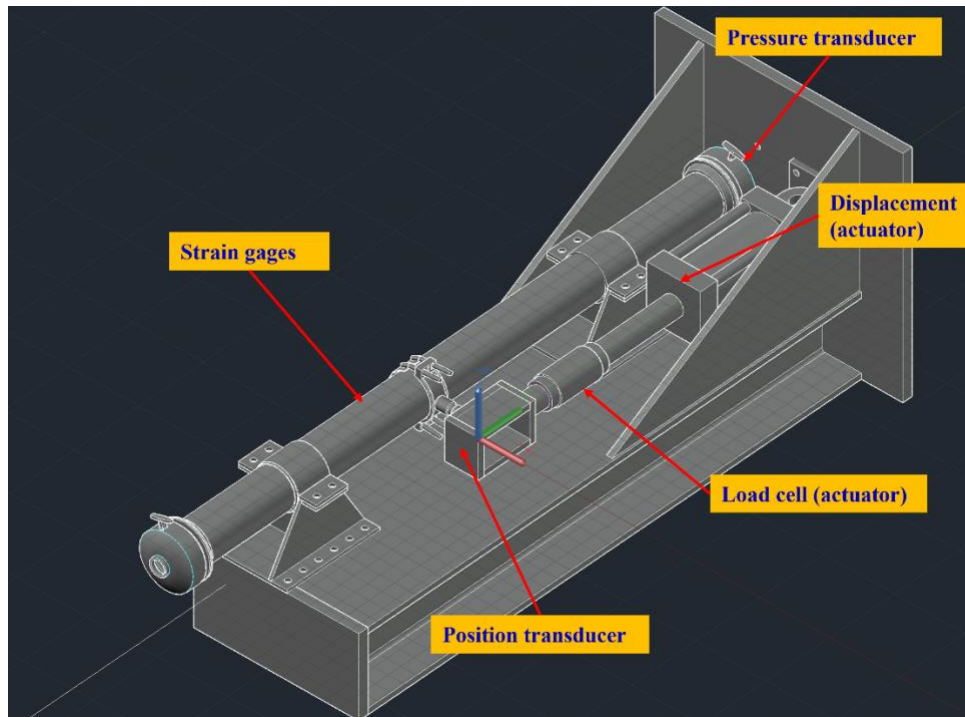


Figure 3-1. Locations of conventional instruments



Figure 3-2. Additional position transducer at saddle

An instrumentation list showing the column number in the data file, name of the channel, description and location for each transducer is presented in Table 3-1.

Table 3-1. Instrumentation list

Data column	Channel name	Description or location
3	Pacific - 1 (0:1:0) actdisp	Actuator displacement
4	Pacific - 2 (0:1:1) load	Actuator force
5	Pacific - 3 (0:1:2) novo1	Saddle displacement
6	Pacific - 4 (0:1:3) press	Water pressure
7	Pacific - 9 (0:2:0)r rgt center	Strain gage (right): center
8	Pacific - 10 (0:2:1) rgt offset	Strain gage (right): circumference
9	Pacific - 11 (0:2:2) rgt circum	Strain gage (right): offset
10	Pacific - 12 (0:2:3) left cente	Strain gage (left): center
11	Pacific - 13 (0:2:4) left offse	Strain gage (left): circumference
12	Pacific - 14 (0:2:5) left circo	Strain gage (left): offset

3.2 LOCATION OF FIBER-OPTIC SENSORS

The NanZee NZS-DSS-C07 fiber-optic cable was installed on both the pipeline and the saddle by the 3M structural plastic adhesive DP8010. Schematic drawings showing the location of the fiber-optic sensors for the benchmark saddle and the PowerSeal saddle are presented in Figure 3-3 and Figure 3-4, respectively. The same piece of the distribution pipeline was used throughout the experimental program and only the saddle was change from test to test. The locations are the same on the pipeline but different on the saddles due to the different designs of two saddles.

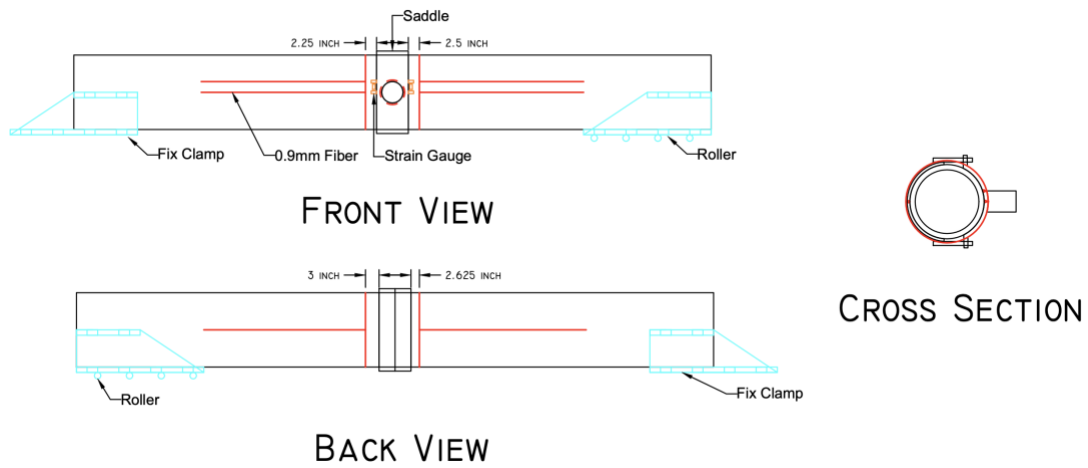


Figure 3-3. Locations of fiber-optic sensors for the Benchmark saddle

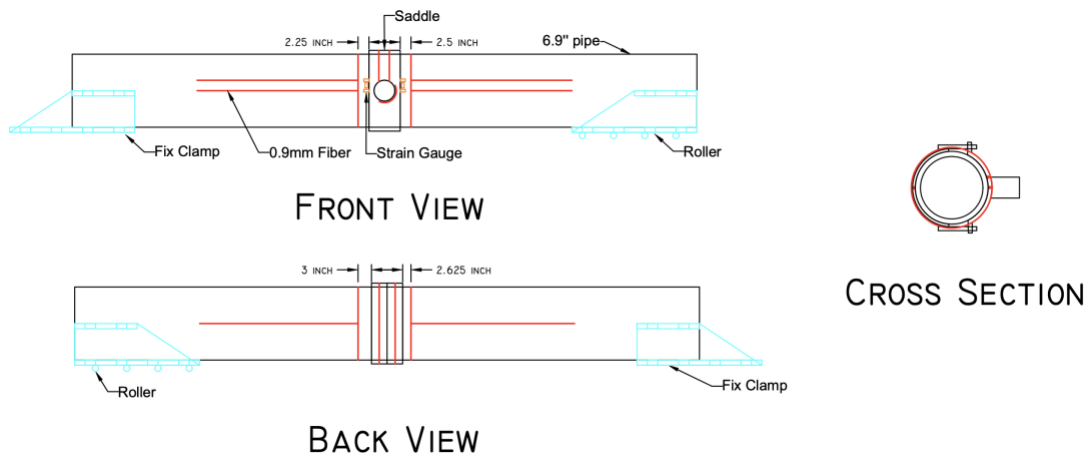


Figure 3-4. Locations of fiber-optic sensors for the PowerSeal saddle

3.3 TEST SPECIMENS

A total of seven tests (three on the conventional saddle and four on PowerSeal saddle) were conducted as listed in Table 3-2. The first saddle from PowerSeal had type 304 straps, shown in Figure 1-1 and listed in the saddle’s specifications in Appendix A. The second and third saddles arrived with straps of another design as presented in Figure 3-5, which have a different design on the connection part between the bolt and the strap. Based on the experiments conducted on these straps, they have a much lower capacity than the ones shown in Figure 1-1. Thus, the straps used on the first test (PS1) were re-used for the second (PS2) and the third (PS3) tests. The performance of PowerSeal saddle with the low-capacity strap was tested in the fourth test (PS2-NewStraps). The performance of PowerSeal saddles was compared to that of the benchmark with the same application of the torque to the nuts pre-tensioning the straps to the pipe. Tests were performed on

three different torque conditions (70, 85 and 100 ft-lb), increased in 15 ft-lb increments starting from the 70 ft-lb as recommended in the specifications [1].

Table 3-2. Test log

Test No	Specimen	Torque (ft-lb)	Test runs	Test date	Note
1	Benchmark1	70	Run872	3/30/2022	
2	Benchmark2	85	Run875	4/19/2022	Fiber-optic sensors were not used.
3	Benchmark3	100	Run878	5/2/2022	
4	PS1	70	Run874	4/8/2022	
5	PS2	85	Run879	5/4/2022	Straps from PS1 were re-used (see Figure 1-1).
6	PS3	100	Run880	5/4/2022	Straps from PS1 were re-used (see Figure 1-1).
7	PS2-NewStraps	85	Run877	5/2/2022	Low-capacity straps were used (see Figure 3-5): type 304 strap

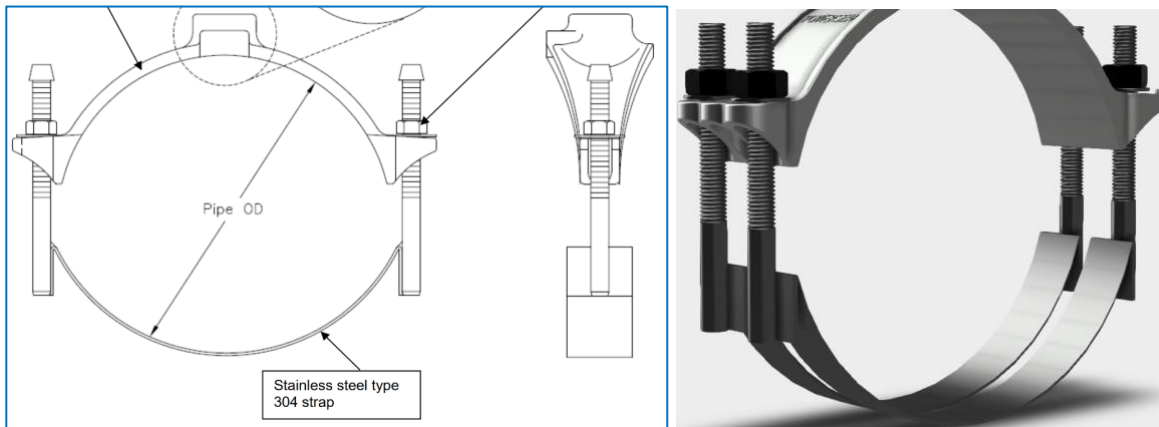


Figure 3-5. Straps with lower capacity

4 Test results of conventional instruments

All test results of conventional instruments are discussed in this section. In addition, this section includes a summary of the typical failure modes and performance parameters of the saddles under the monotonic shear loading.

4.1 TEST DATA ANALYSIS

For a given applied torque, a monotonic pull parallel to the longitudinal axis of the pipeline was applied. The tests were conducted up to failure of the saddle or a significant water leak. This report summarized peak values of the force and the respective displacement at maximum force obtained from the test data. The test results are provided in pairs for each torque value comparing the saddle from PowerSeal to the benchmark. The results for the torque at 70 ft-lb are shown in Figure 4-1. The results for 85 ft-lb and 100 ft-lb torque values are shown in Figure 4-2 and Figure 4-3, respectively. The results for PowerSeal saddles with different straps at 85 ft-lb torque are shown in Figure 4-4.

It is worth noting that the maximum forces in the benchmark tests are closely correlated to a significant pressure drop because of the saddle's failure in shear. The pressure drop in the case of the PowerSeal saddles is less noticeable at the first leak, because it started from a few drops and gradually increased during the test.

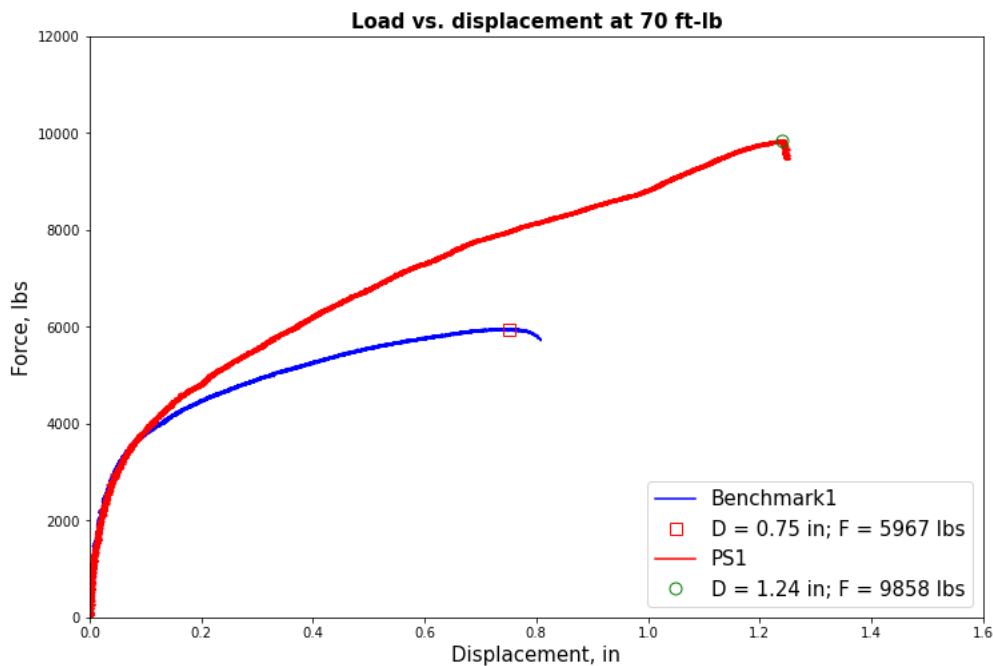


Figure 4-1. Test results for 70 ft-lb torque

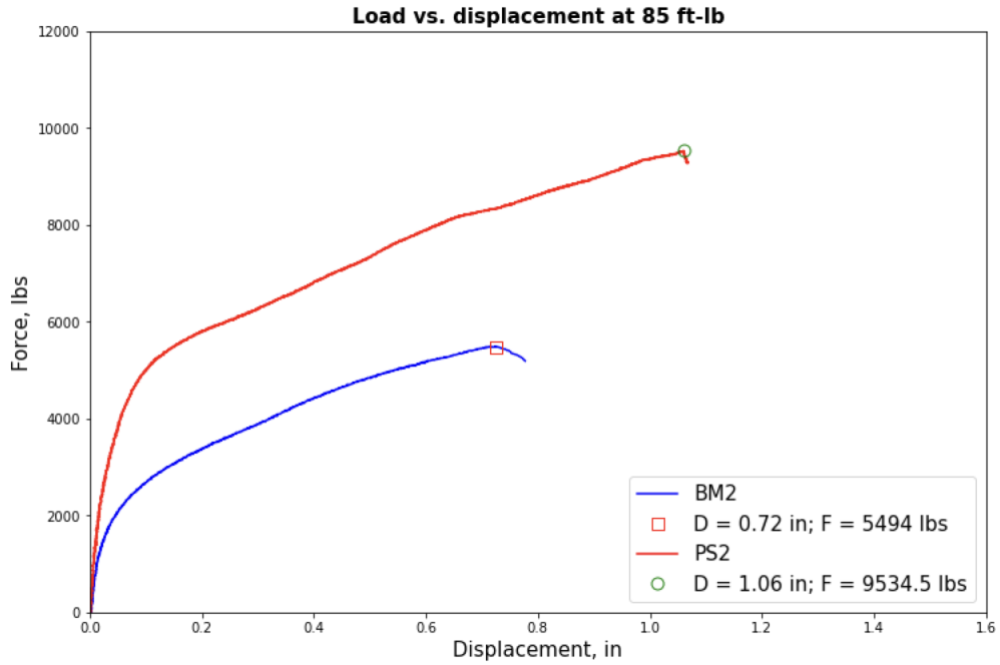


Figure 4-2. Test results for 85 ft-lb torque

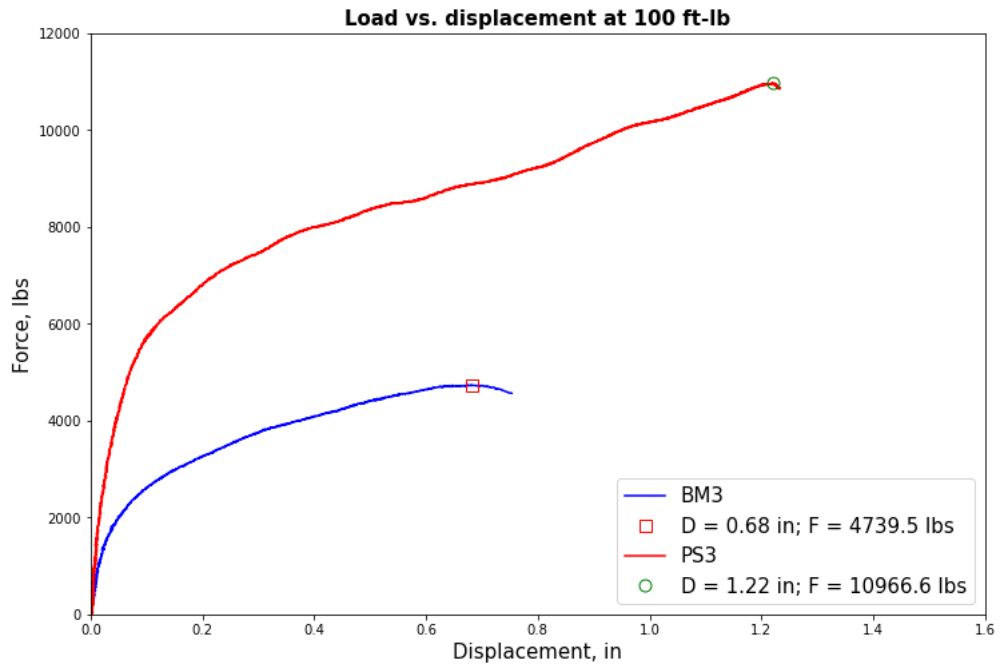


Figure 4-3. Test results for 100 ft-lb torque

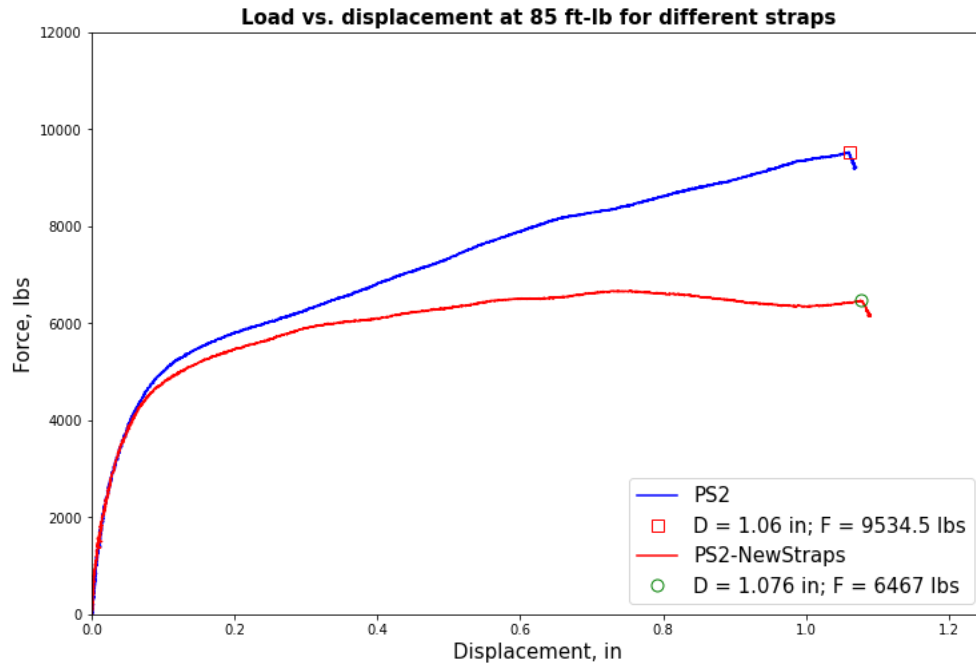


Figure 4-4. Test results for PowerSeal saddles with different straps at 85 ft-lb torque

4.2 FAILURE MODES

The failure modes of the benchmark and the PowerSeal saddles were completely different from one another. The tests on the benchmark saddles were stopped because of the failure of the saddle and an explosive water release as presented in Figure 4-5. The force dropped right after the failure for the benchmark saddle cases.



Figure 4-5. Typical failure of benchmark saddle

Water leaked from the PowerSeal saddles started at a level of a few drips as presented in Figure 4-6. The testing of the PowerSeal saddles was stopped when the gradually increasing water leak turned into a significant leak (at which the maximum force was recorded). It is worth noting that the benchmark saddle was completely sheared off, whereas the PowerSeal saddles just slid off the pipe.



Figure 4-6. PowerSeal saddle: dripping water leak close to the maximum force

4.3 COMPARATIVE SUMMARY OF TEST DATA

A summary of the test results obtained for the benchmark saddles is presented in Table 4-1. The average of the maximum force is 5400 lbs. with a coefficient of variation (COV) of 11.5%. The respective displacement at the maximum load has a lower COV of about 4.9% with an average of 0.72 in.

Table 4-1. Summary of test results for benchmark saddle

Specimen	Torque (ft-lb)	Test runs	D@F _{max} , in	F _{max} , lbs.
Benchmark1	70	Run872	0.75	5967
Benchmark2	85	Run875	0.72	5494
Benchmark3	100	Run878	0.68	4739.5
		Mean:	0.72	5400
		STD:	0.04	619
		COV, %:	4.9%	11.5%

A summary of the test results obtained for the PowerSeal saddles is shown in Table 4-2. The average of the maximum force is 10119.7 lbs. with a coefficient of variation (COV) of 7.4%. The respective displacement at the maximum load has COV of 8.4% with an average of 1.17 in.

Table 4-2. Summary of test results for PowerSeal saddle

Specimen	Torque (ft-lb)	Test runs	D@F _{max} , in	F _{max} , lb
PS1	70	Run874	1.24	9858
PS2	85	Run879	1.06	9534.5
PS3	100	Run880	1.22	10966.6
Mean:			1.17	10119.7
STD:			0.1	751
COV, %:			8.4%	7.4%

A displacement normalized to that of the benchmark at 70 ft-lb torque is presented in Figure 4-7. Results show that the PowerSeal saddle has at least a 40% higher displacement capacity than the conventional saddle. A maximum force normalized to that of the benchmark at 70 ft-lb torque is shown in Figure 4-8. The PowerSeal saddle has at least a 60% greater force capacity than the conventional saddle. The PowerSeal saddle did not fail in a dramatic way. An explosive water leak happened in the case of the benchmark saddle.

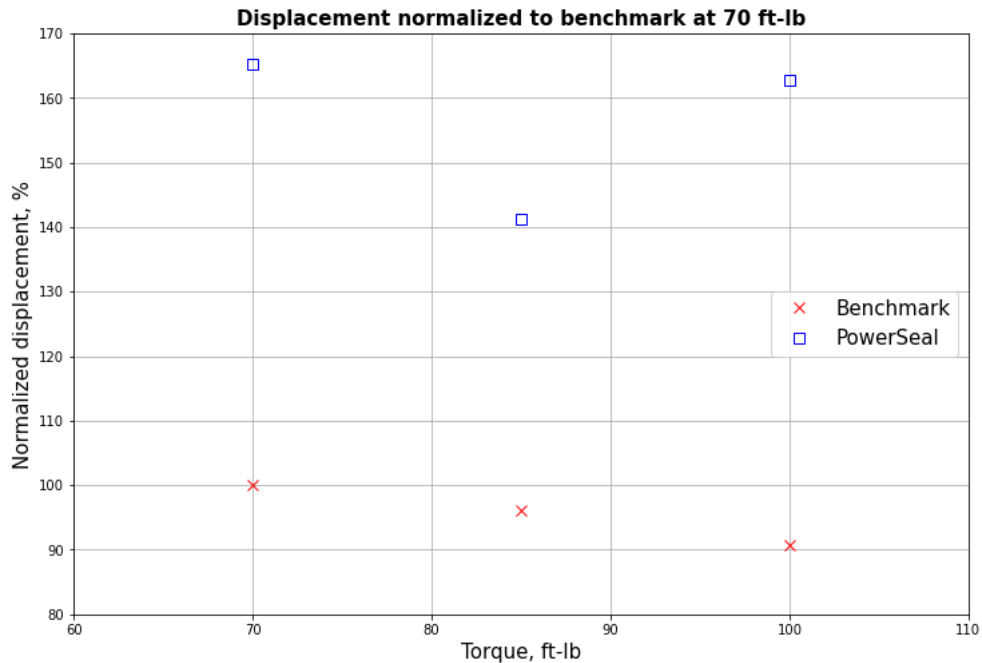


Figure 4-7. Normalized displacement

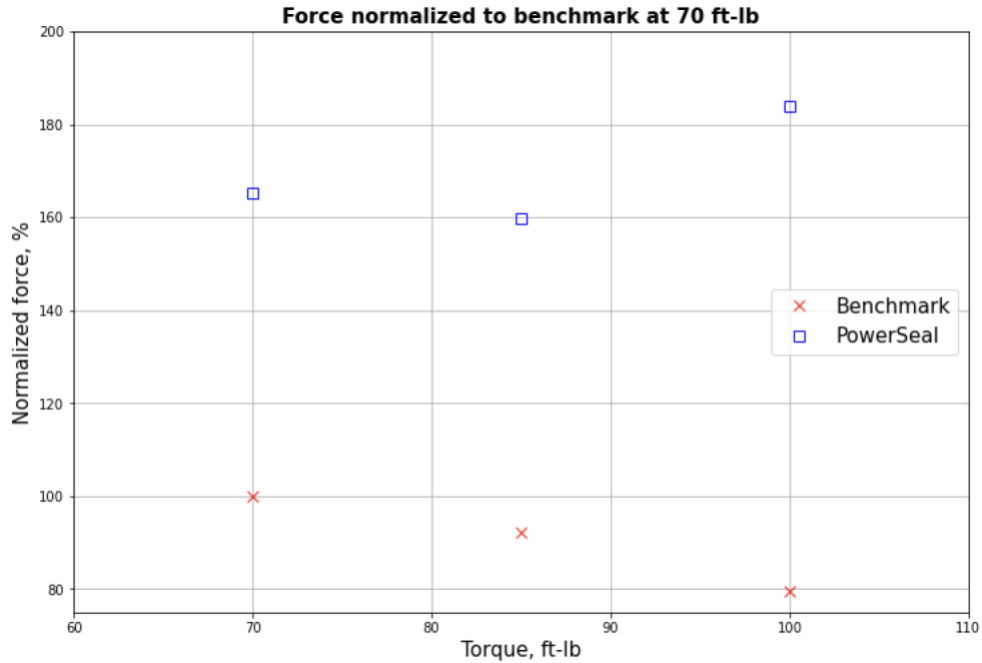


Figure 4-8. Normalized force

A summary of the test results obtained for the PowerSeal saddles with original straps and low-capacity straps is shown in Table 4-3. With the same torque value (85 ft-lb), results show that the PowerSeal saddle with the original straps (PS2) has similar displacement capacities but 47% greater force capacity than the one with the low-capacity straps (PS2-NewStraps).

Table 4-3. Summary of test results for PowerSeal saddles with different straps

Specimen	Torque (ft-lb)	Test runs	D@F _{max} , in	F _{max} , lb
PS2	85	Run879	1.06	9534.5
PS2-NewStraps	85	Run877	1.076	6467.0

5 Test results of fiber-optic sensors

All test results of fiber-optic sensors are discussed in this section.

5.1 TEST DATA ANALYSIS

LUNA ODiSI 6104 Optical Distributed Sensor Interrogator (LUNA) was used in the tests. The settings for LUNA in each test are presented in Table 5-1. More details about LUNA and distributed fiber-optic sensing are provided in Appendix C.

Table 5-1. Setting for LUNA

Test No	Specimen	Torque (ft-lb)	Test runs	Test date	Gage pitch (mm)	Measurement Rate (Hz)
1	Benchmark1	70	Run872	3/30/2022	0.65	6.25
2	Benchmark2	85	Run875	4/19/2022	N/A	N/A
3	Benchmark3	100	Run878	5/2/2022	0.65	6.25
4	PS1	70	Run874	4/8/2022	0.65	4.167
5	PS2	85	Run879	5/4/2022	1.3	8.333
6	PS3	100	Run880	5/4/2022	1.3	8.333
7	PS2-NewStraps	85	Run877	5/2/2022	0.65	4.167

For the convenience of data processing, the fiber-optic cables were indexed by segments. The index for Benchmark1 and Benchmark3 is presented in Figure 5-1. The index for PS1 is presented in Figure 5-2. The index for PS2, PS3, and PS4 is presented in Figure 5-3. In this section, all the indices will refer to the ones shown in Figure 5-3.

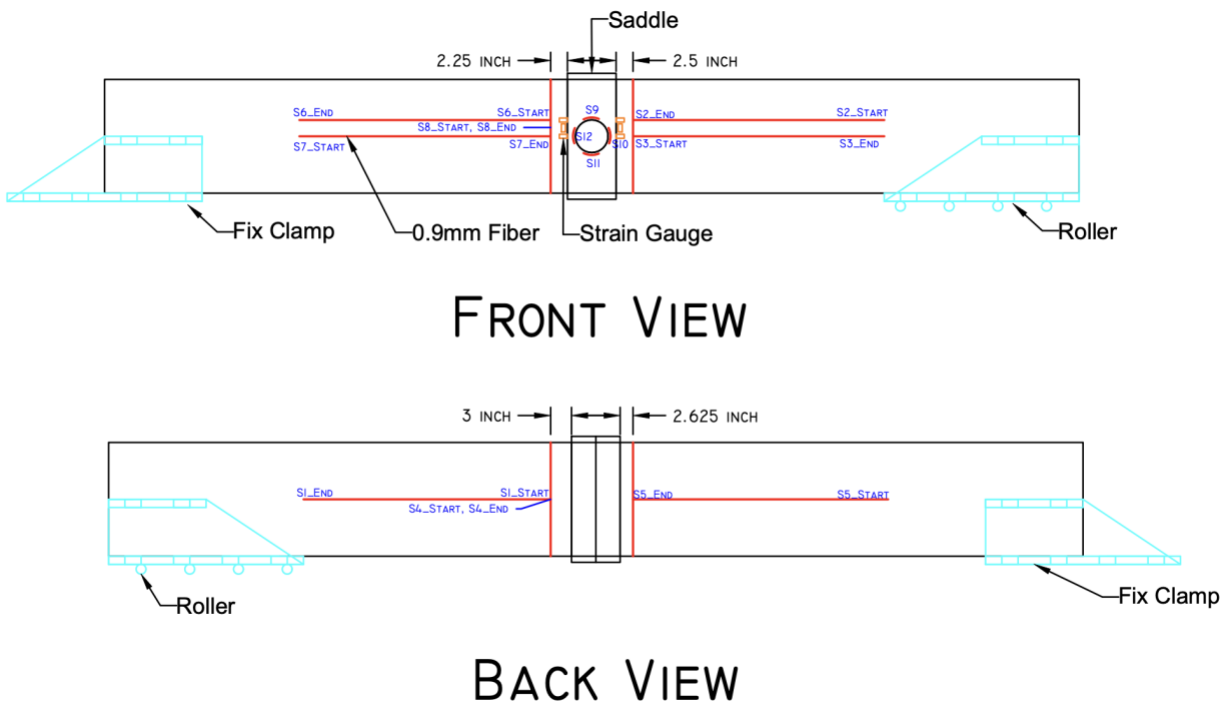
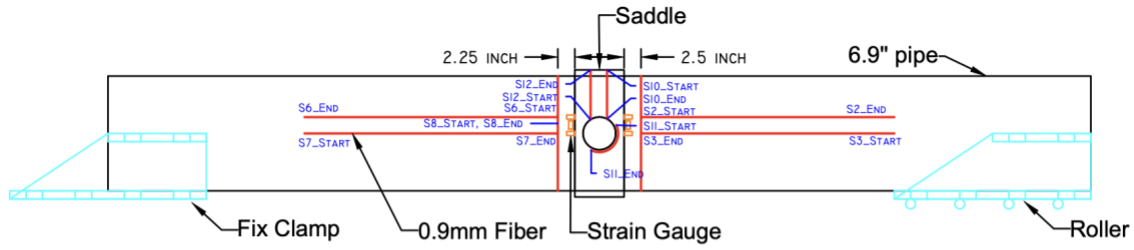
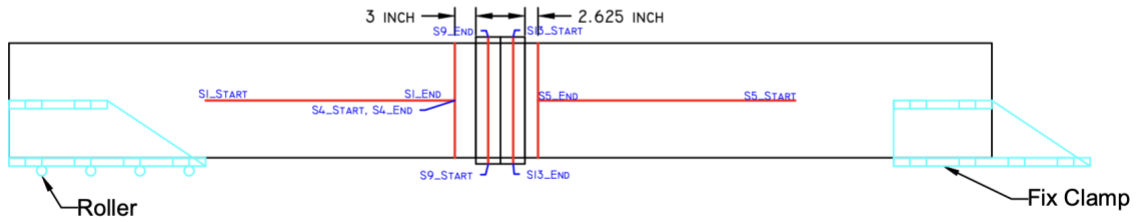


Figure 5-1. Index for the fiber-optic cables for Benchmark1 and Benchmark3

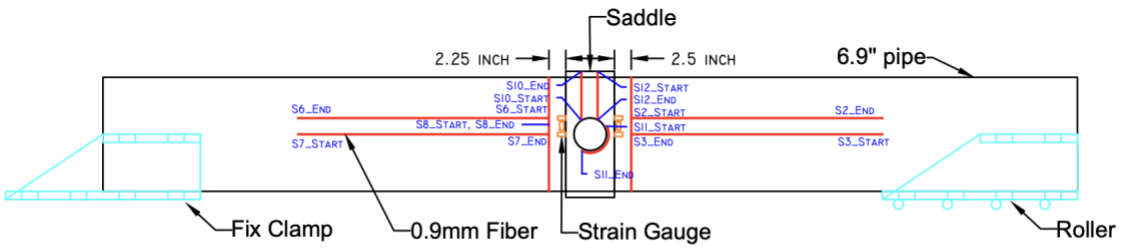


FRONT VIEW

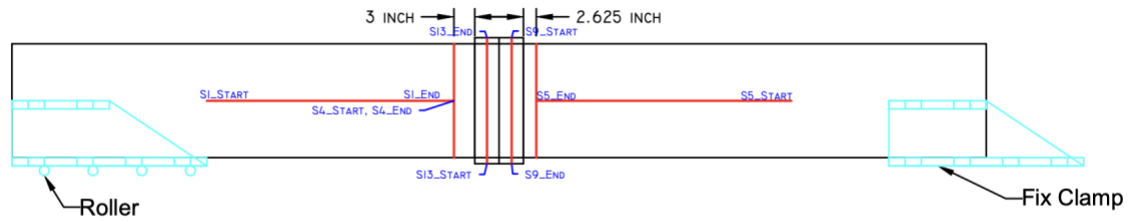


BACK VIEW

Figure 5-2. Index for the fiber-optic cables for PS1



FRONT VIEW



BACK VIEW

Figure 5-3. Index for the fiber-optic cables for PS2, PS3, and PS4

The fiber-optic data collected from Sensor 7, Sensor 8, and Sensor 13 are compared and analyzed in this report. Sensor 7 was installed along the longitudinal direction of the pipeline (Figure 5-4). Sensor 8 was installed along the circumferential direction of the pipeline (Figure 5-5). Sensor 13 was installed on the strap (Figure 5-6). The test results of all fiber-optic sensors are provided in Appendix D.

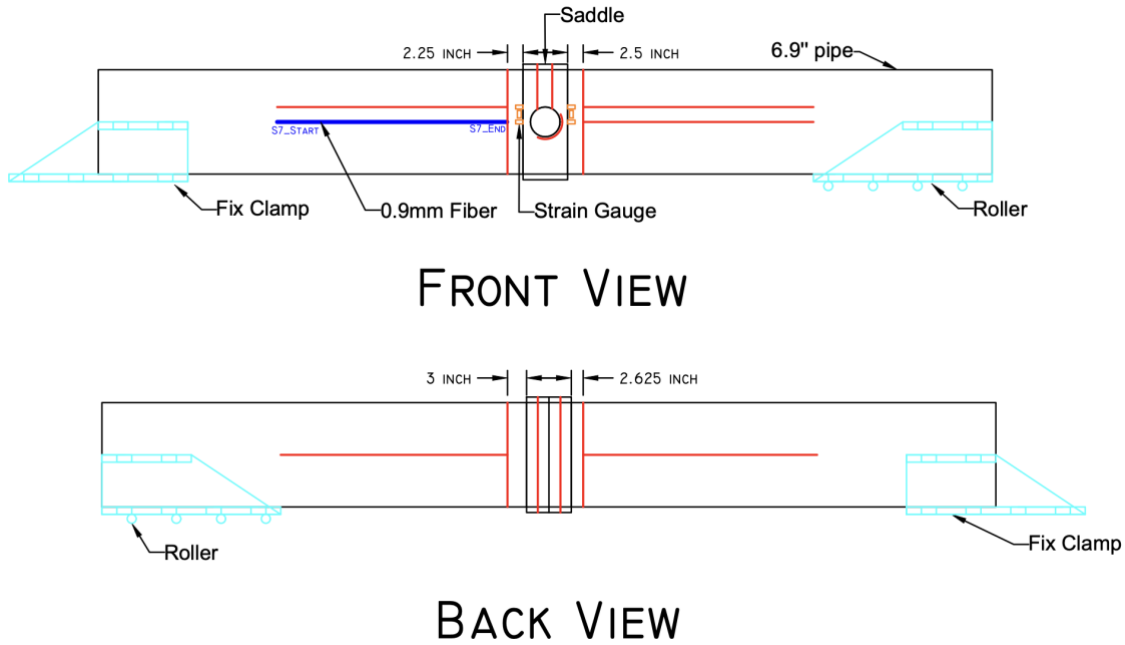


Figure 5-4. Location of Sensor 7 (the blue segment along the longitudinal direction of the pipeline)

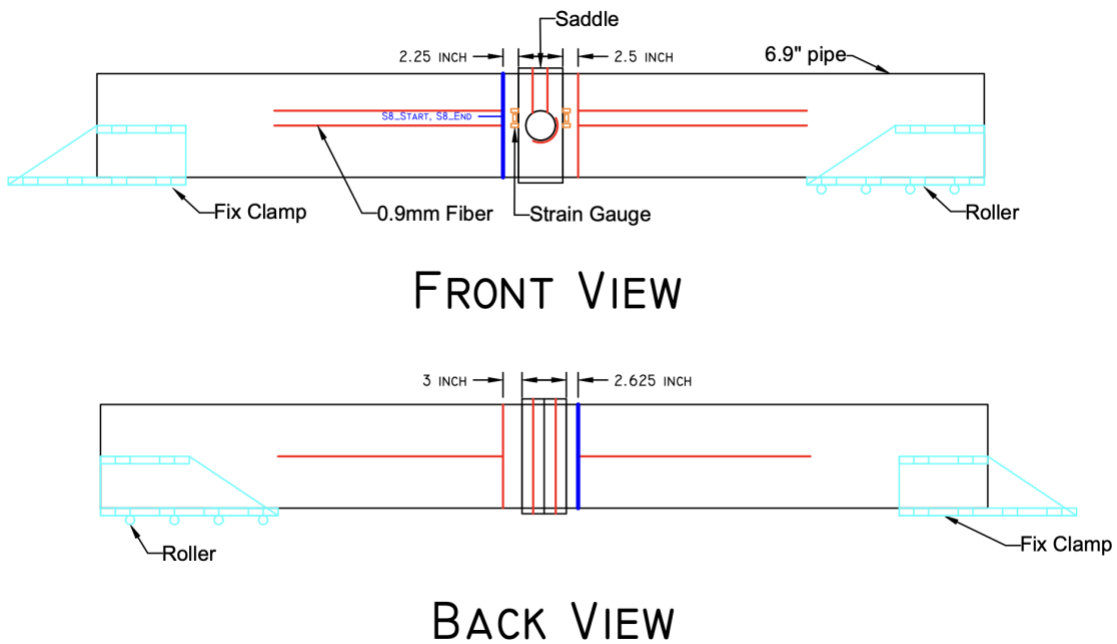


Figure 5-5. Location of Sensor 8 (the blue segment along the circumferential direction of the pipeline)

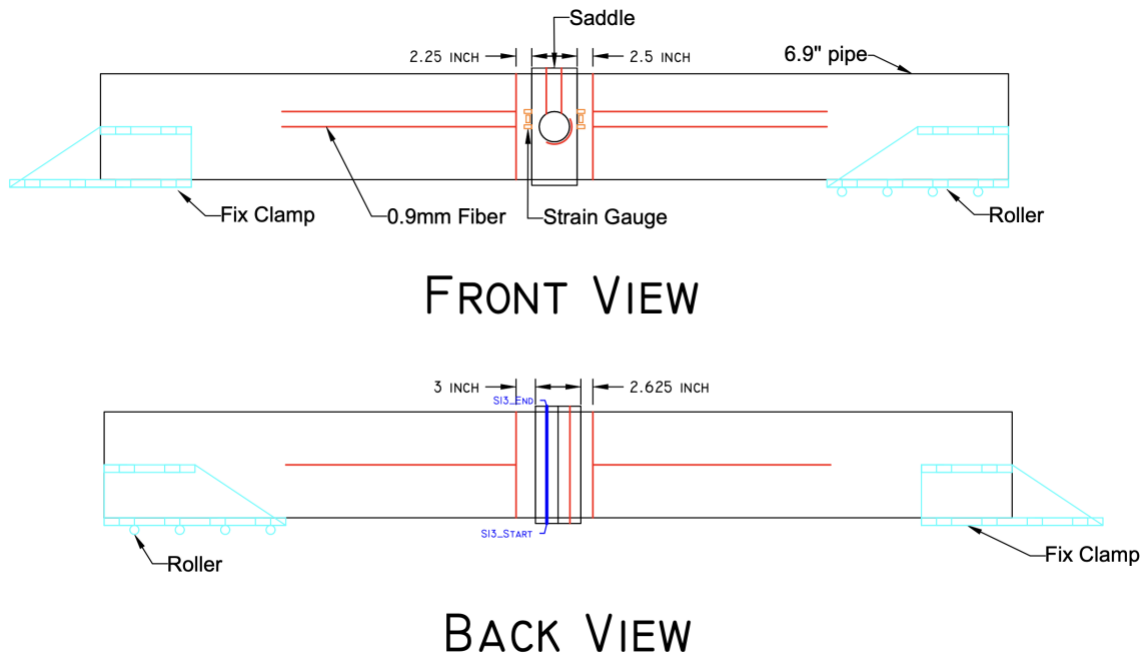


Figure 5-6. Location of Sensor 13 (the blue segment on the strap)

5.1.1 Comparison between strain gage and fiber-optic data

The strain gage and fiber-optic data collected from BM1 in both longitudinal and circumferential directions are compared and analyzed to validate the reliability of the fiber-optic data.

In the longitudinal direction, the end point of Sensor 7 is compared with the strain gage (Pacific - 9 (0:2:0)r rgt center). The result is presented in Figure 5-7.

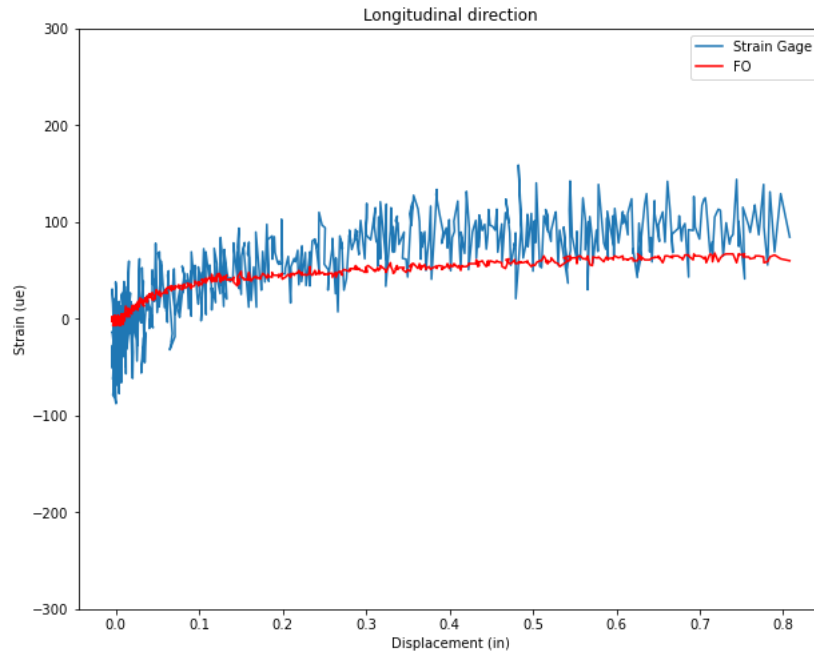


Figure 5-7. Comparison between the strain gage and fiber-optic data in the longitudinal direction on the pipeline

In the circumferential direction, the start point of Sensor 8 is compared with the strain gage (Pacific - 11 (0:2:2) rgt circum). The result is presented in Figure 5-8.

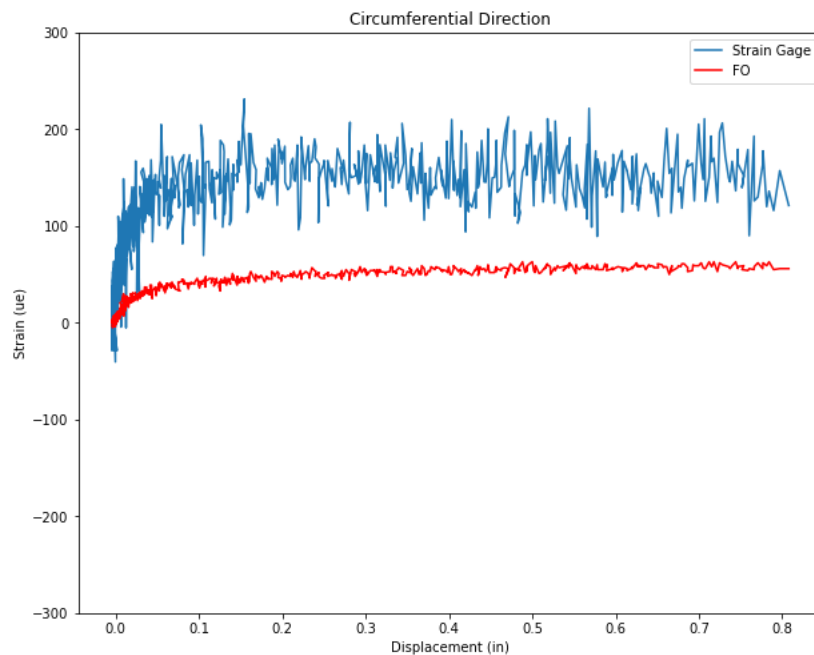


Figure 5-8. Comparison between the strain gage and fiber-optic data in the circumferential direction on the pipeline

It can be found that in both longitudinal and circumferential directions, the fiber-optic data has similar trends as the strain gage data but with smaller magnitudes, which might be mainly due to the different locations of the fiber-optic sensors and strain gages. In order to avoid the large bending angle of the fiber-optic cable, the end point of Sensor 7 and the start point of Sensor 8 were installed more than 2 inches away from the saddle. While the strain gages do not have this limitation, they were intentionally installed much closer to the saddle, which were about 0.5 inches away from the saddle (Figure 5-9). Thus, it is expected that the strain gages would measure larger strains than the fiber-optic sensors.

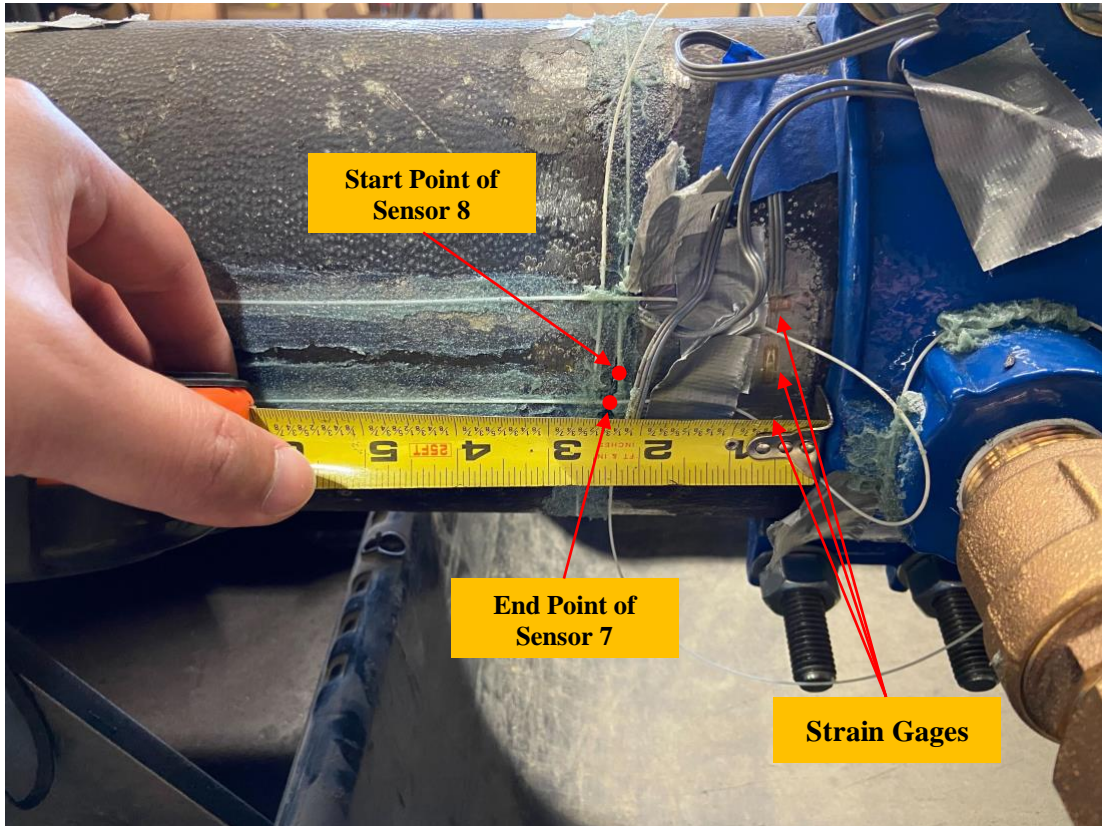


Figure 5-9. Locations of strain gages and the data points of fiber-optic sensors for BM1

5.1.2 Comparison between benchmark and PowerSeal saddles

The fiber-optic data of benchmark and PowerSeal saddles are compared and analyzed here to further access their performance under the monotonic shear loading. Because the fiber-optic cable installations on two saddles are different, only the results of the fiber-optic sensors on the pipeline (Sensor 7 and Sensor 8) of Benchmark1 and PS1 are compared herein.

The results of the strain distribution on Sensor 7 at loading of 5500 lbs. for Benchmark 1 and PS1 are shown in Figure 5-10. The results of the maximum strains changing with the loading and displacement on Sensor 7 for the two tests are shown in Figure 5-11. It can be found that, in the longitudinal direction, before Benchmark1 failed, the strain distributions and the maximum

strain developments on the pipeline were very similar for Benchmark1 and PS1. In addition, the strain on the pipeline would become larger when it got closer to the saddle.

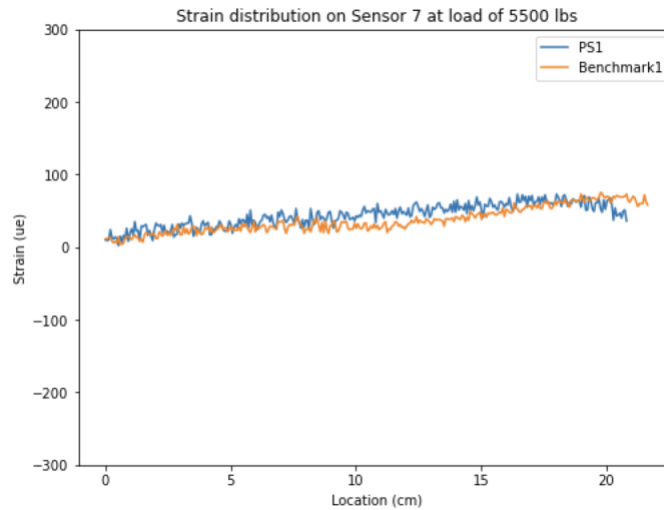


Figure 5-10. Strain distribution on Sensor 7 at load of 5500 lbs.

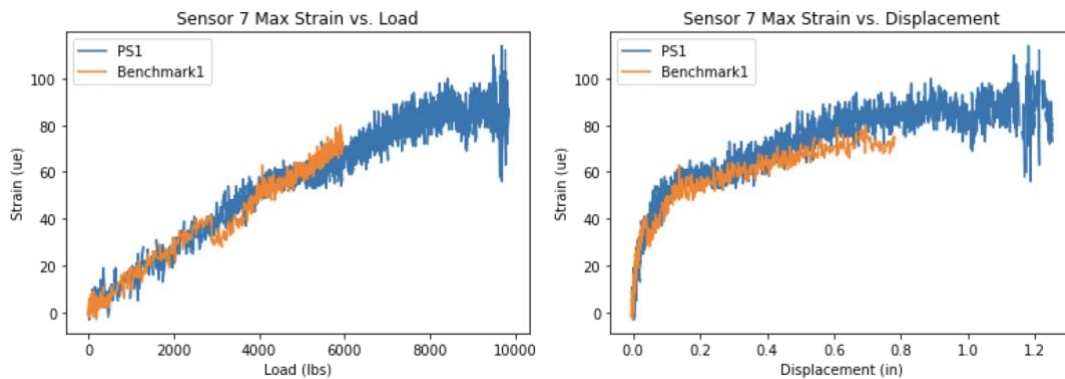


Figure 5-11. Maximum strain on Sensor 7

The results of the strain distribution on Sensor 8 at loading of 5500 lbs. for Benchmark1 and PS1 are shown in Figure 5-12. The results of the maximum and minimum strains changing with the loading and displacement on Sensor 8 for the two tests are shown in Figure 5-13. In the circumferential direction, the strain distributions and the maximum and minimum strain developments on the pipeline also had very similar trends for the two tests, but the strains for Benchmark1 were slightly larger than the ones for PS1 in terms of the magnitude before Benchmark1 failed. In addition, it is worth noting that as the start point and end point of Sensor 8 were both at the middle of the pipeline in the front (Figure 5-5), it can be found that, the pipeline would experience tension on the front and back of the pipeline, and compression on the top and bottom of the pipeline in its circumferential direction (Figure 5-14). It indicated that the pipeline was slightly squeezed by the saddle along its latitudinal axis while the saddle was pulled monotonically.

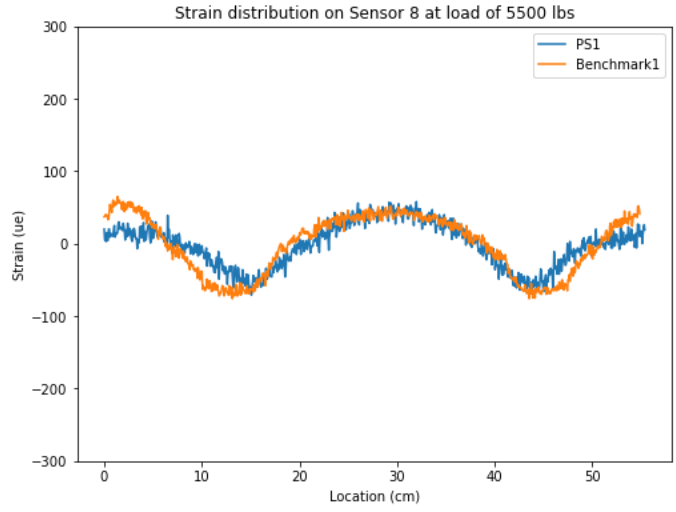


Figure 5-12. Strain distribution on Sensor 8 at load of 5500 lbs.

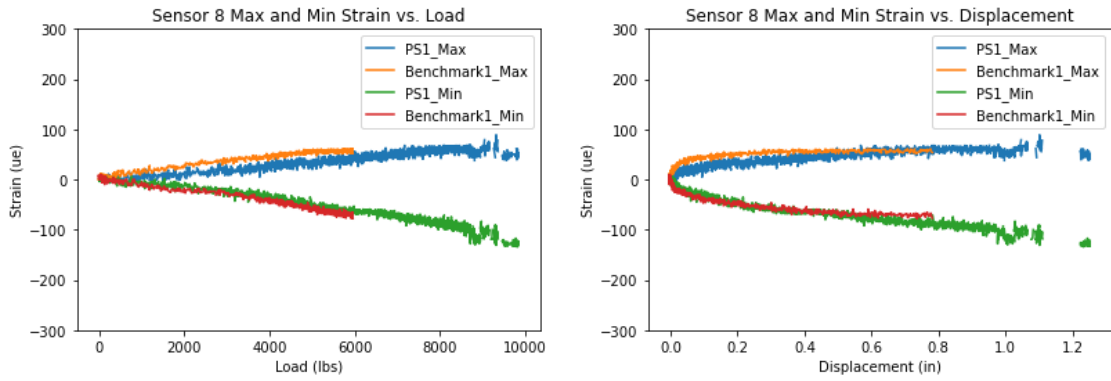


Figure 5-13. Maximum and minimum strain on Sensor 8

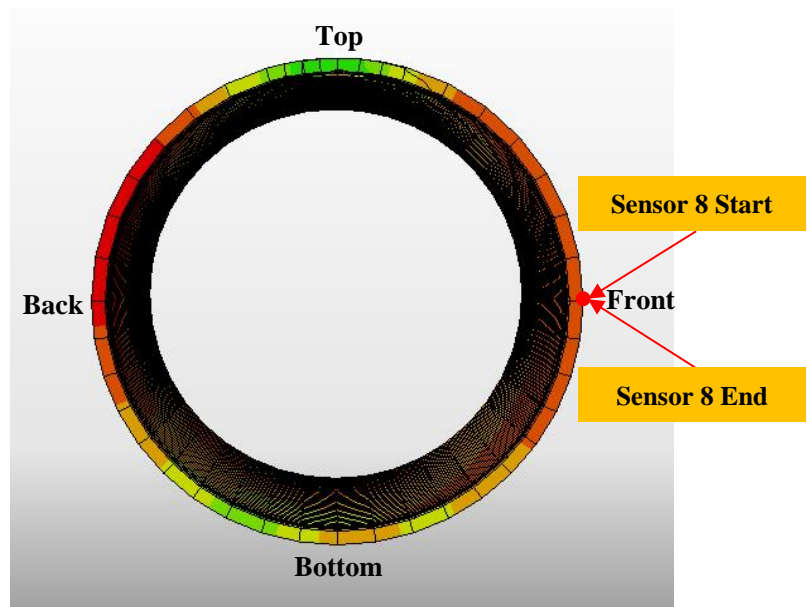


Figure 5-14. Cross-section of the pipeline

5.1.3 Comparison of PowerSeal saddles with different torques

Fiber-optic results of the PowerSeal saddles under three different torque conditions (70 ft-lb, 85 ft-lb, and 100 ft-lb) are compared and analyzed in this section.

The results of the strain distribution on Sensor 7 at loading of 9000 lbs. for PS1 (70 ft-lb), PS2 (85 ft-lb), and PS3 (100 ft-lb) are shown in Figure 5-15. The results of the maximum strains changing with the loading and displacement on Sensor 7 for three tests are shown in Figure 5-16. The results of the strain distribution on Sensor 8 at loading of 9000 lbs. for PS1, PS2, and PS3 are shown in Figure 5-17. The results of the maximum strains changing with the loading and displacement on Sensor 8 for three tests are shown in Figure 5-18, and the results of the minimum strains are shown in Figure 5-19.

It is worth noting that in the longitudinal direction, the strain distributions on the pipeline for three tests were very similar. However, under the same loading and displacement conditions, the saddle with smaller torques would lead to larger maximum strains on the pipeline. In the circumferential direction, the strain distributions and the maximum and minimum strain developments on the pipeline had very similar trends, but the saddle with smaller torques would cause larger strains on the pipeline in terms of the magnitude. It might be because the saddle with smaller torques would have a larger rotating angle θ under the monotonic pulling, which would create a larger moment on the pipeline and result in larger strains on the side opposite to the pulling direction (Figure 5-20).

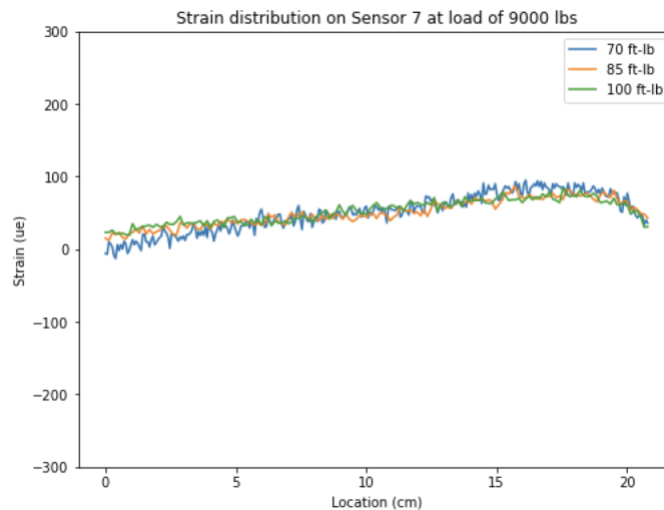


Figure 5-15. Strain distribution on Sensor 7 at load of 9000 lbs.

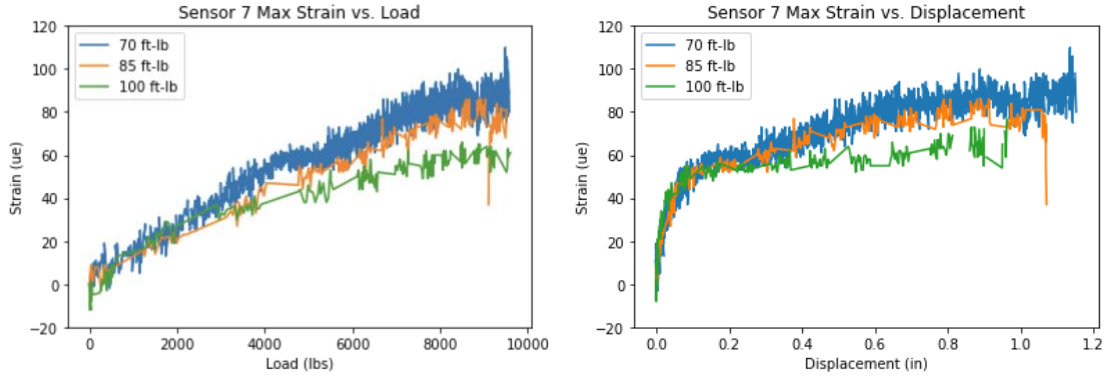


Figure 5-16. Maximum strain on Sensor 7

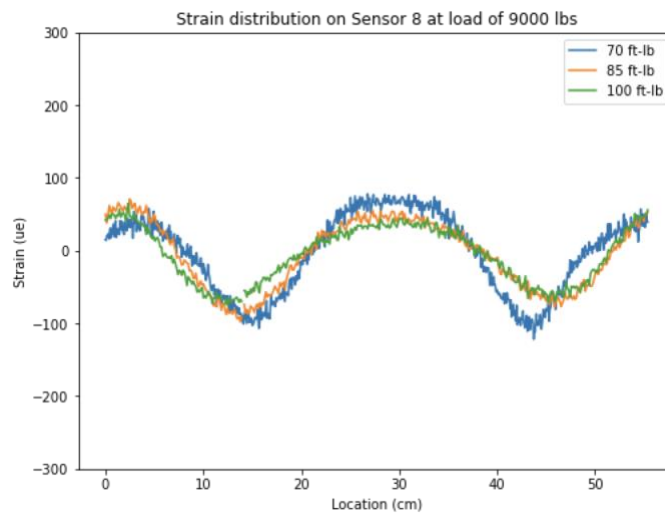


Figure 5-17. Strain distribution on Sensor 8 at load of 9000 lbs.

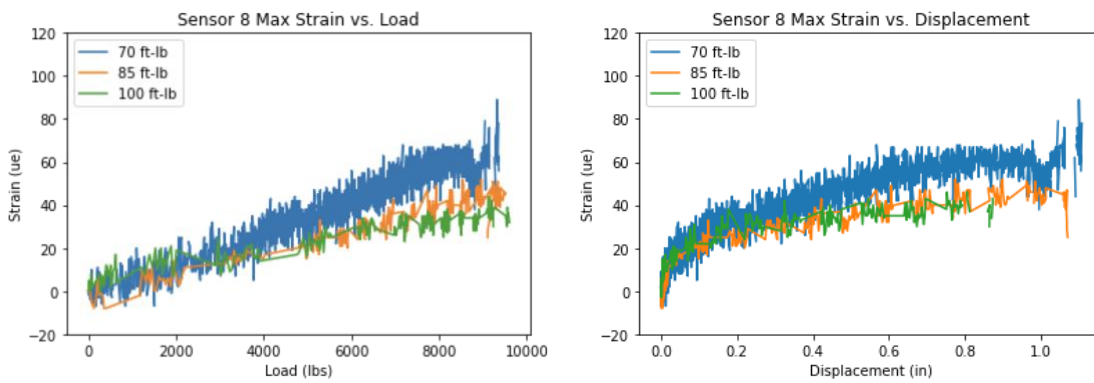


Figure 5-18. Maximum strain on Sensor 8

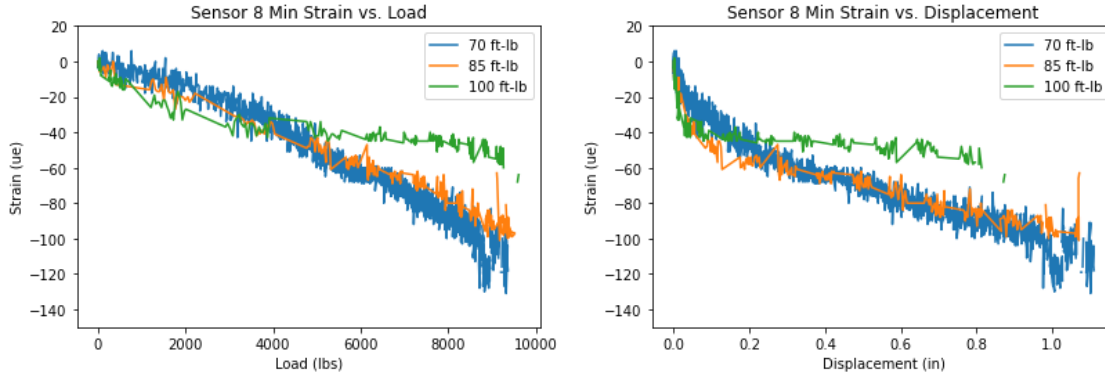


Figure 5-19. Minimum strain on Sensor 8

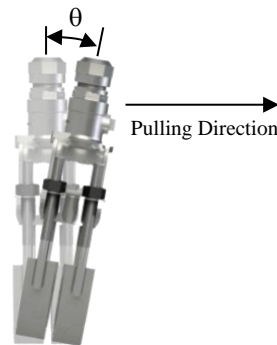


Figure 5-20. Rotation of the saddle under pulling

The results of the strain distribution on Sensor 13 at loading of 9000 lbs. for PS1 (70 ft-lb), PS2 (85 ft-lb), and PS3 (100 ft-lb) are shown in Figure 5-21. The results of the maximum strains changing with the loading and displacement on Sensor 13 for three tests are shown in Figure 5-22. On the saddle, it can be noticed that compared to the ones for PS1 and PS3, the strain distribution for PS2 had a similar trend but a much smaller magnitude. It might be because the fiber-optic cables were not fully stucked on the straps in this test. As a result, PS2 also had a smaller maximum strain than PS1 and PS3 when the load and displacement increased. Besides, for PS1 and PS3, it can be found that the magnitudes of two peaks were different, where the strap experienced a larger tension on its top side. It indicated that the saddle might have an offset upwards under the monotonic shear loading. Also, for a given displacement, PS3 would have a larger maximum strain than PS1, which is because PS3 experienced greater axial load than PS1.

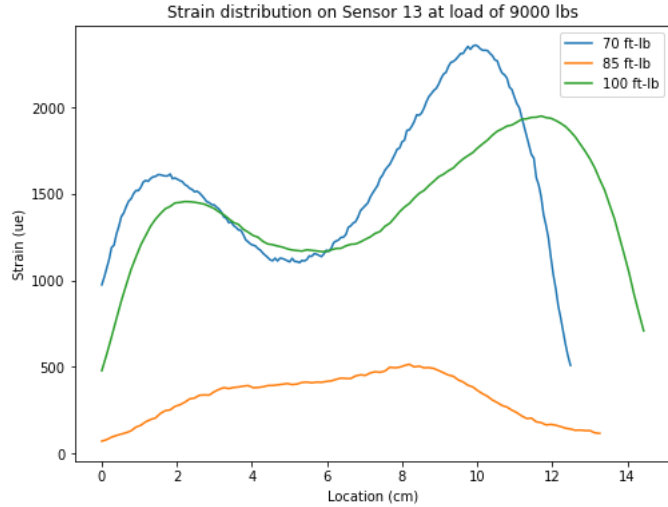


Figure 5-21. Strain distribution on Sensor 13 at load of 9000 lbs.

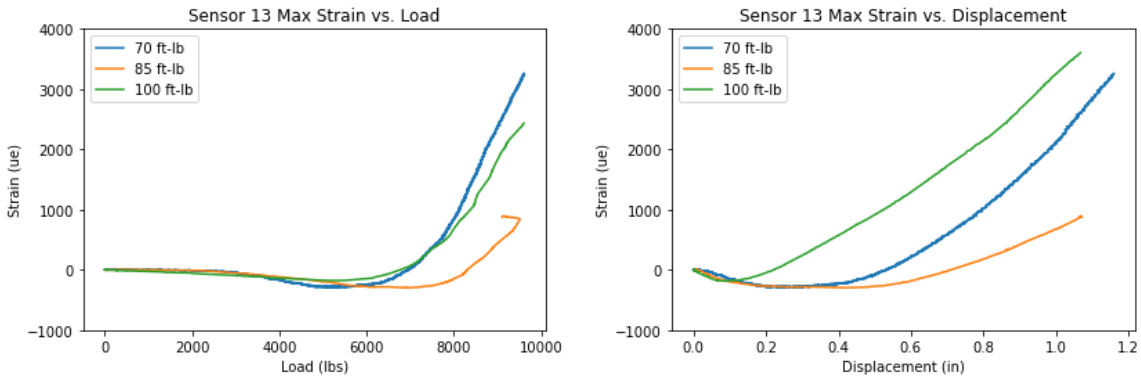


Figure 5-22. Maximum strain on Sensor 13

5.1.4 Comparison of PowerSeal saddles with different straps

Fiber-optic results of PowerSeal saddles with different straps (original straps and low-capacity straps) are compared and analyzed to assess the impact of these two kinds of straps.

The results of the strain distribution on Sensor 7 at loading of 9000 lbs. for PS2 (with original straps) and PS2-New Straps (with low-capacity straps) are shown in Figure 5-23. The results of the maximum strains changing with the loading and displacement on Sensor 7 for the two tests are shown in Figure 5-24. In the longitudinal direction, PS2 (with original straps) would cause a larger strain on the pipeline under the monotonic shear loading.

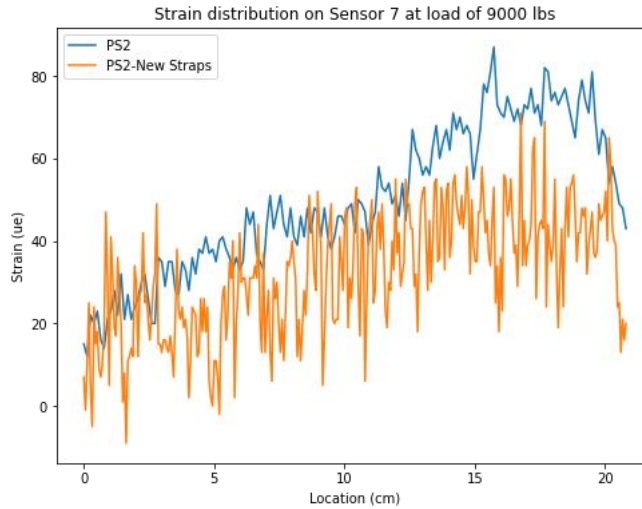


Figure 5-23. Strain distribution on Sensor 7 at load of 9000 lbs.

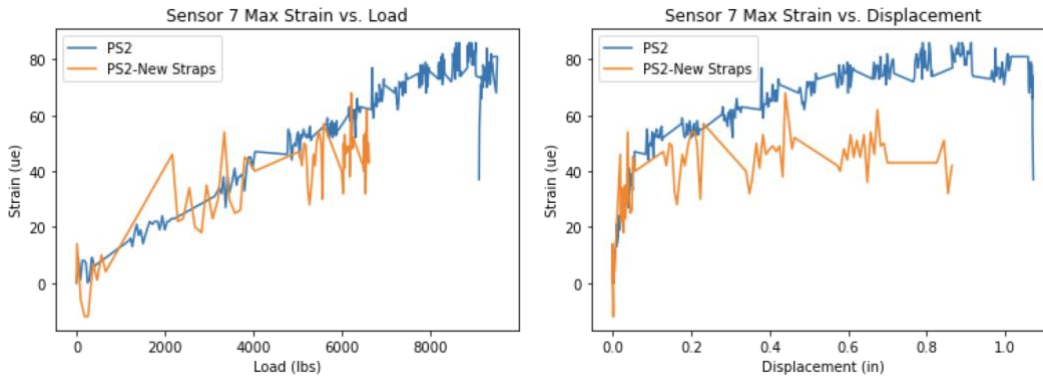


Figure 5-24. Maximum strain on Sensor 7

The results of the strain distribution on Sensor 8 at loading of 9000 lbs. for PS2 (with original straps) and PS2-New Straps (with low-capacity straps) are shown in Figure 5-25. The results of the maximum strains changing with the loading and displacement on Sensor 8 for the two tests are shown in Figure 5-26. In the circumferential direction, PS2 (with original straps) would cause a larger strain on the pipeline in terms of the magnitude under the monotonic shear loading.

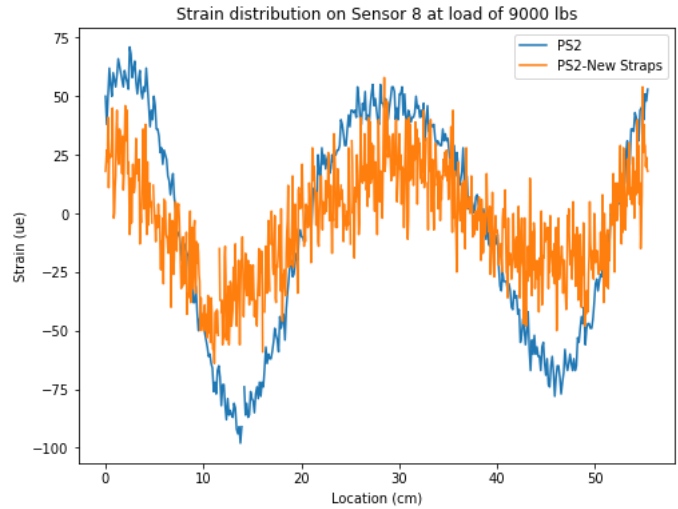


Figure 5-25. Strain distribution on Sensor 8 at load of 9000 lbs.

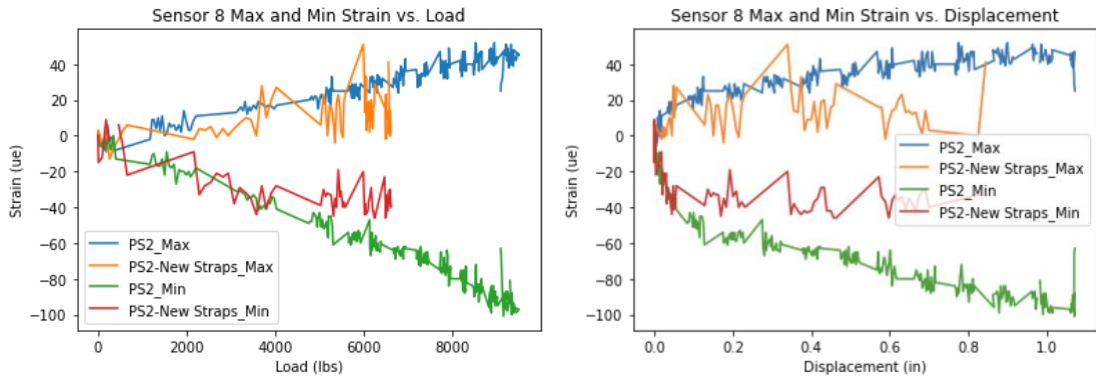


Figure 5-26. Maximum strain on Sensor 8

The results of the strain distribution on Sensor 13 at loading of 9000 lbs. for PS2 (with original straps) and PS2-New Straps (with low-capacity straps) are shown in Figure 5-27. The results of the maximum strains changing with the loading and displacement on Sensor 13 for the two tests are shown in Figure 5-28. On the straps, it was worth noting that PS2-New Straps would have a very different strain distribution trend than PS2, which would experience compression on the bottom side and tension on the top side. PS2-New Straps would also experience larger maximum strains than PS2 under the same loading and displacement conditions.

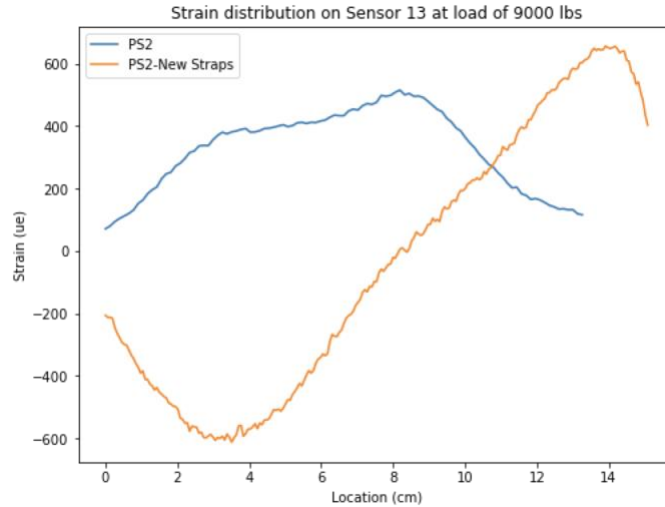


Figure 5-27. Strain distribution on Sensor 13 at load of 9000 lbs.

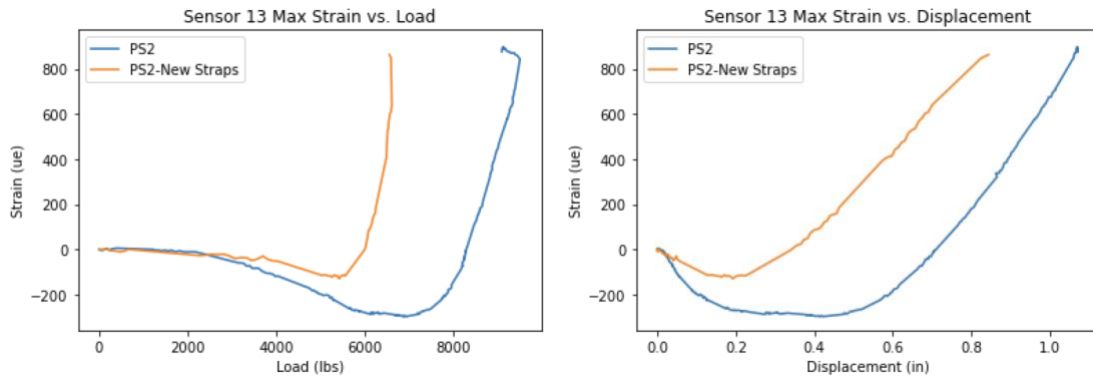


Figure 5-28. Maximum strain on Sensor 13

6 Finite Element Analysis

6.1 OVERVIEW OF NUMERICAL MODEL

The finite element analysis was conducted to examine the behavior of the PowerSeal saddle and the pipeline under monotonic shear loading using ABAQUS software [2]. The geometries of the saddle and the pipe models were generated to match the experimental setup. The isotropic 3D solid continuum element (C3D8R) is used for the finite element meshes in the analysis (Figure

6-1). The number of elements and nodes in the finite element model (FEM) are 203,875 and 173,796, respectively.

The boundary and loading conditions are briefly summarized as follows. One pipe end was fixed in X, Y, Z directions, while another end of the pipe was allowed to move horizontally in z direction as the lab test. The FEM enables contacting and sliding interactions between the pipe and the saddle. The normal behavior of the interaction is set as hard contact in ABAQUS, and the friction coefficient of the tangential behavior is set as 0.5 according to the standard friction coefficient between materials of ductile iron and stainless steel [3].

The modeling process begins with applying an 85-ft-lb torque on each bolt. 70 psi water pressure was applied on the inner surface of the pipe. Then the shear loading was applied on the saddle with 3 inches displacement. This FEM was used to verify PS2 (PowerSeal saddle with 85-ft-lb torque on the bolts).

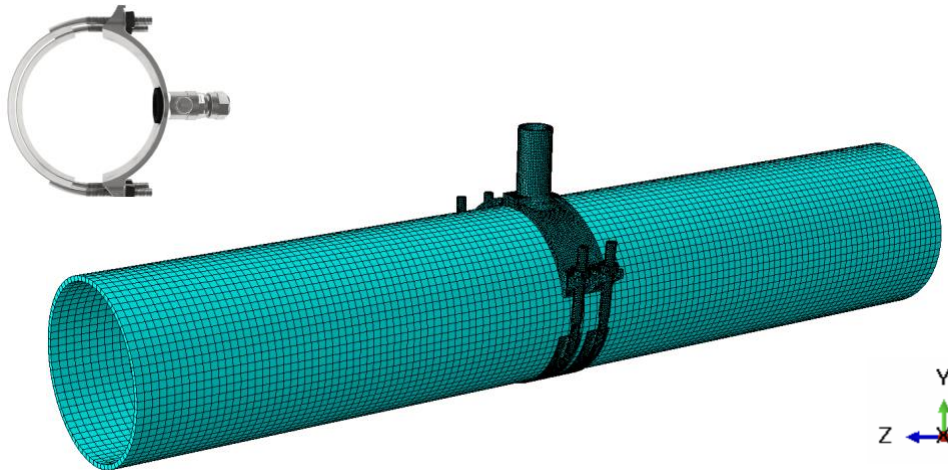


Figure 6-1 3-D FE model mesh for saddle test

6.2 DETERMINATION OF RUBBER INTERFACE

The rubber interface between saddle and pipe is modelled using a series of coupled spring elements to reduce computation cost with little effect on result accuracy as shown in Figure 6-2. The spring stiffness in normal and tangential directions were calculated based on the properties of the nitrile rubber (NBR) used for the PowerSeal saddle.

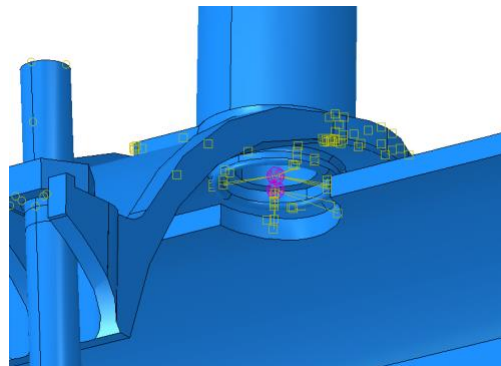


Figure 6-2 Coupled spring model

The spring stiffness was calculated as follows using Hook law.

$$\Delta f = k \cdot \Delta x = \Delta \sigma \cdot A = \Delta \varepsilon \cdot E \cdot A$$

$$\Delta \varepsilon = \frac{\Delta x}{h}$$

$$k \cdot \Delta x = \frac{\Delta x}{h} \cdot E \cdot A$$

$$k = \frac{EA}{h} = \frac{\pi(d_2^2 - d_1^2)E}{4h}$$

where E is the young’s modulus; A is the rubber interface area; h is thickness of the rubber; d₁ and d₂ are the inner and outer diameters of the rubber respectively; k is the spring stiffness calculated by Hook law: $\Delta f = k \cdot \Delta x$.

6.3 DETERMINATION OF MATERIAL PARAMETERS

Plastic properties are included in case the yielding stress is reached.

Table 6-1 presents the material properties of the ductile iron pipe and saddle used in the tests. Plastic properties are included in case the yielding stress is reached.

Table 6-1. Material parameters

Part	Density (lb./in ³)	Young’s Modulus (psi)	Poisson’s Ratio	Yield Strength (psi)	Ultimate Strength (psi)	Elongation
Ductile Iron Pipe (plastic)	0.28	23,500,000	0.29	42,000	60,000	10%
Saddle steel (elastic)	0.286	25,700,000	0.3	N/A	N/A	N/A

6.4 FEM RESULTS & DISCUSSIONS

6.4.1 Overview of FE analysis

Figure 6-3 shows the Mises stress contour of the pipe and saddle when the displacement reaches 1.1 inches where the water leakage initiated in the lab test. The maximum Mises stress

was found around the strap and the connection area between the bolts and the straps. Besides, when the applied shear loading was increasing, the left area on each strap will be detached from the pipe.

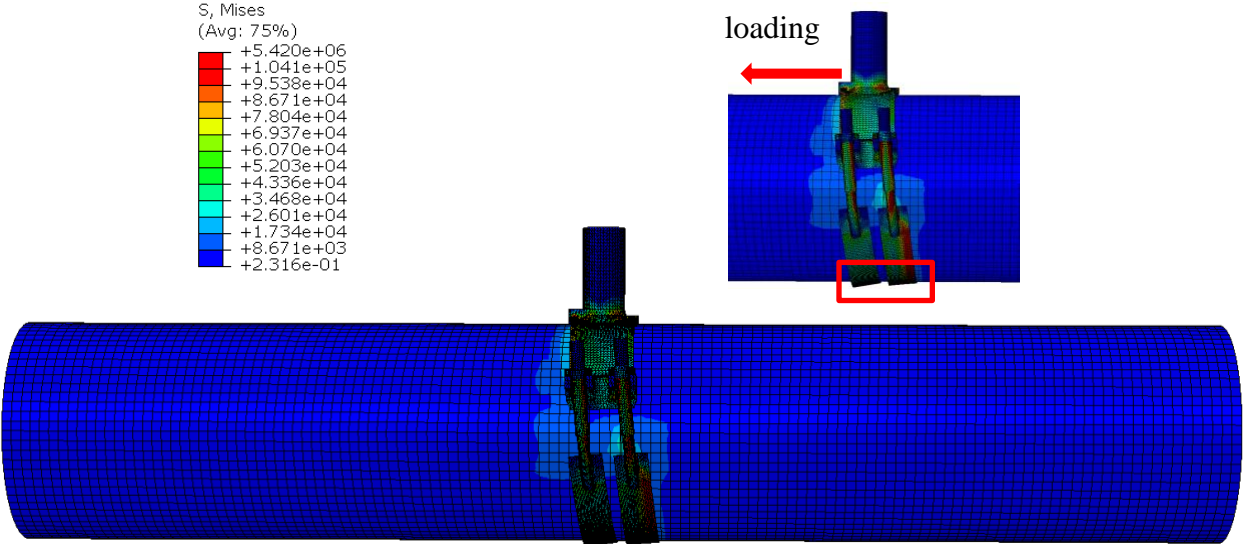


Figure 6-3 Coupled spring interaction model

6.4.2 Comparison of the FEM results and experimental fiber-optic data

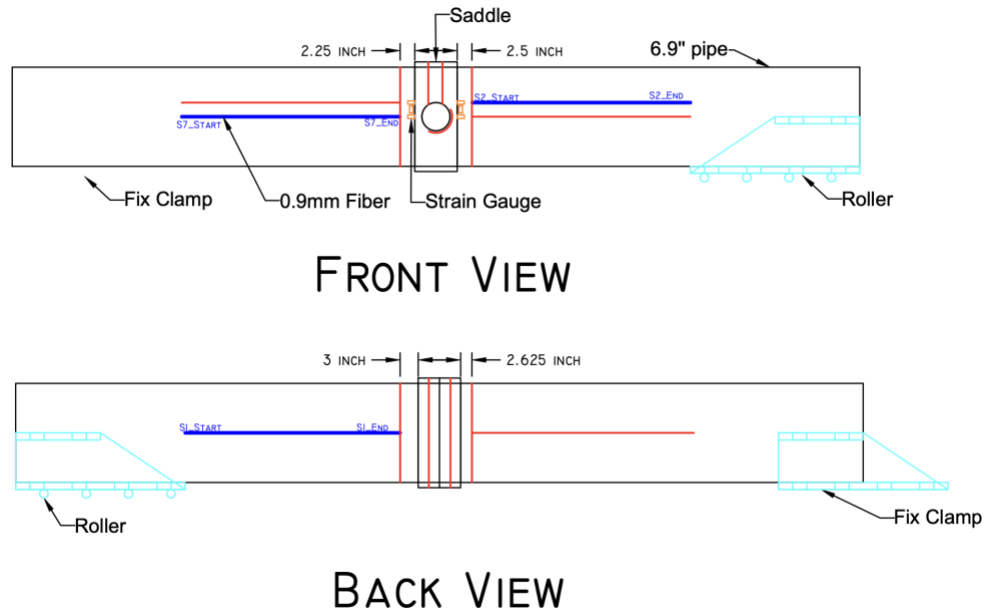


Figure 6-4 and Figure 6-5 indicate the locations of longitudinal and circumferential sensors on the pipe.

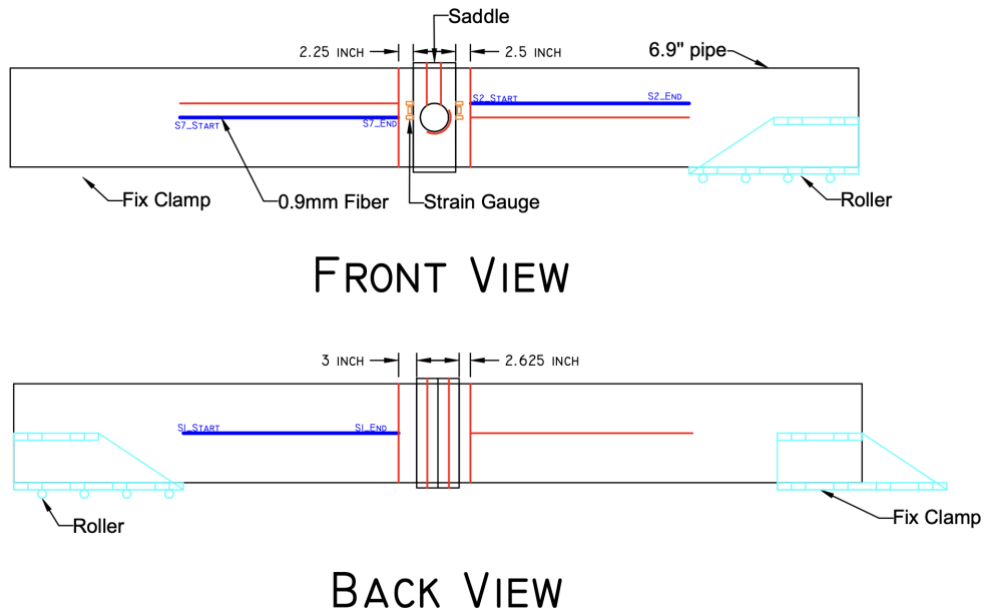


Figure 6-4 Location of longitudinal sensors on the pipe: S1, S2, S7 (the blue segment along the longitudinal direction of the pipeline)

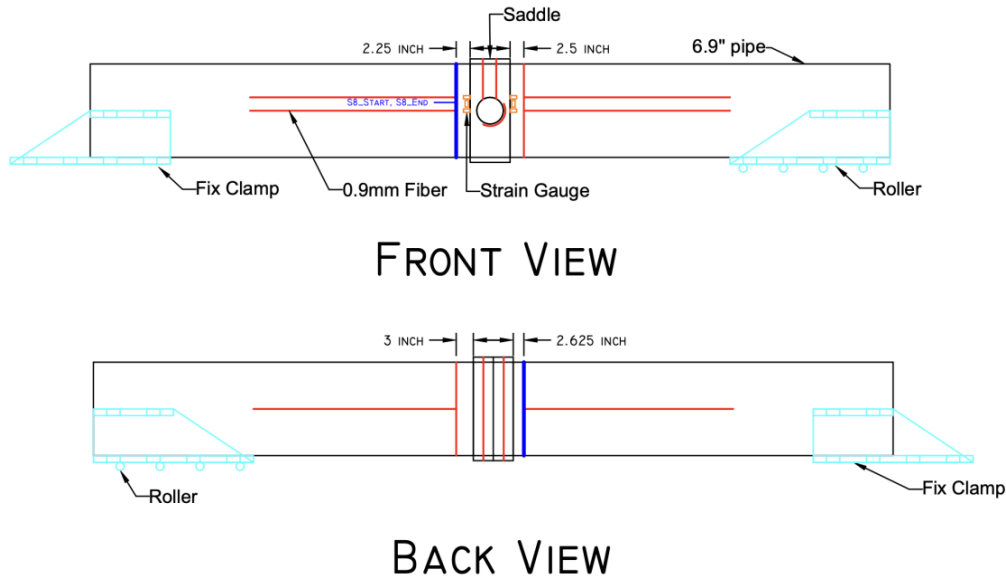
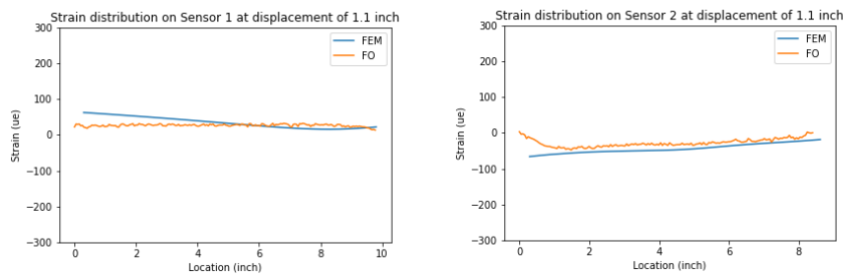


Figure 6-5 Location of circumferential sensor on the pipe: S8 (the blue segment along the circumferential direction of the pipeline)

Figure 6-6 shows the comparison of longitudinal strain on the pipe from the FEM results and fiber-optic (FO) data. Sensor 1, Sensor 2, and Sensor 7 measured the longitudinal strain along the pipeline, and Sensor 8 measures the circumferential strain of the pipeline near the saddle. The FEM results overall match the FO data. Both the FEM and FO results show that the strain on Sensor 1 and Sensor 7 were in tension, and Sensor 2 was in compression. Sensor 8 indicates that the pipe was squashed in the transverse cross-sectional plane. Theoretically, the total strain obtained is mainly consisted of shear force-induced strain and moment-induced strain. As it can be found from the plots, the strain values in FEM are always higher than that of FO strain, which might be because the fiber-optic sensors were not installed in an ideal way, where some parts were not tightly attached on the surface.



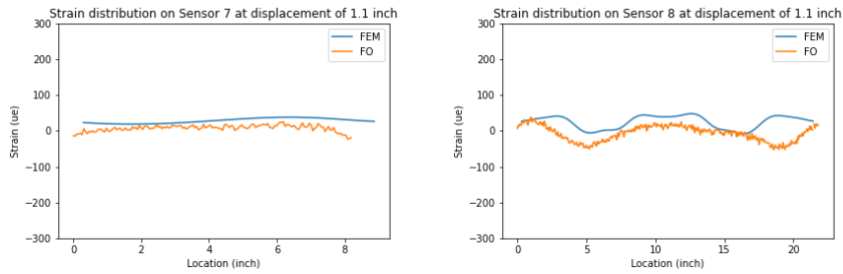
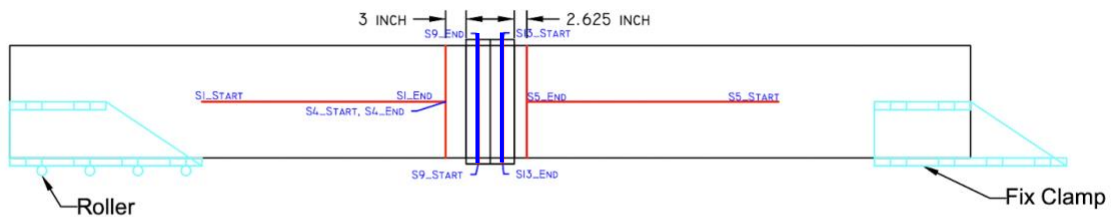


Figure 6-6 Comparison of strains on the pipe

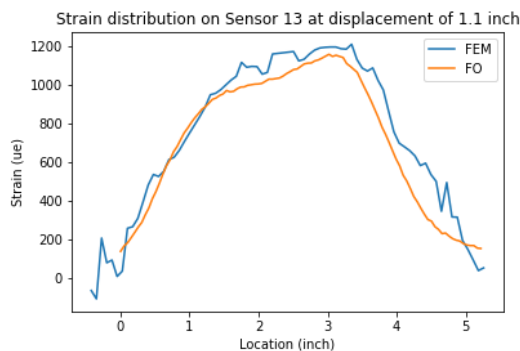
Figure 6-7 shows the locations of corresponding sensors on the saddle straps.



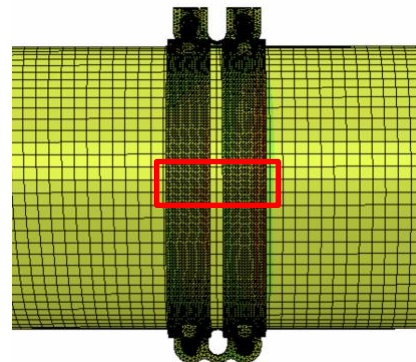
BACK VIEW

Figure 6-7 Locations of circumferential sensors on the saddle straps: S9 and S13 (the blue segment along the circumferential direction of the pipeline)

It can be observed from Figure 6-8(a) that the strap was under tension as simulated by the FEM. The strain from two ends of the strap to the center is increasing and the maximum strain peak around $1200 \mu\epsilon$ near the center. It is reasonable because the middle area of strap as shown in Figure 6-8(b) was fully contacted to the pipe compared to the ends of strap.



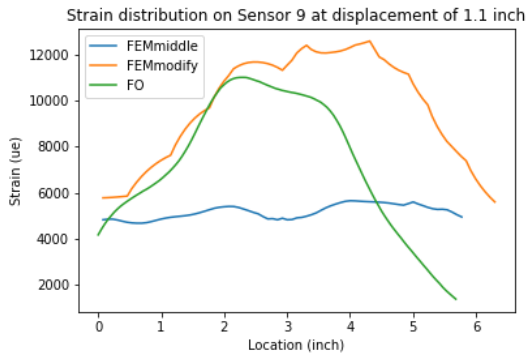
(a)



(b)

Figure 6-8 (a) Comparison of strain of S13; (b) Back view of saddle setup

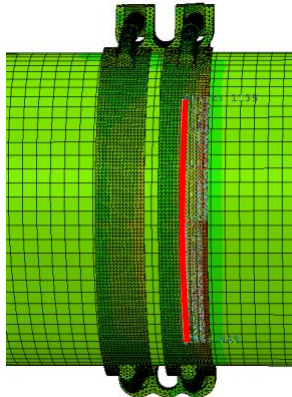
In Figure 6-9(a), the blue line (FEMmiddle) represents the circumferential strain in the midline of the strap. Although the trend can be matched between FO and FEMmiddle, there is a difference of the strain magnitude. The reason could be that the location of Sensor 9 may not be attached as straight as expected, and a tiny location difference could lead to non-negligible strain differences. Therefore, a different path was simulated (Figure 6-9 (d)) and the results can basically match the FO data.



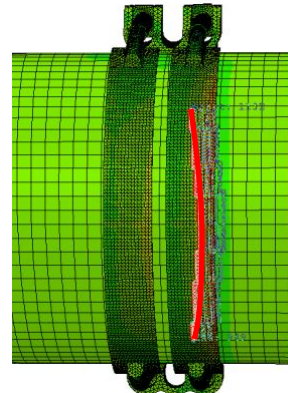
(a)



(b)



(c)



(d)

Figure 6-9 (a) Comparison of strain of S9; (b) Circumferential strain plot on strap; (c) Strain path of the FEM-middle; (d) Strain path of FEM-modify

7 Conclusions

This report discusses the results of the experimental program focused on the performance of service saddles under monotonic shear loading. A performance of the service saddles from PowerSeal was compared to that of the benchmark saddle. Based on the test results of conventional instruments, the following was concluded. First, the PowerSeal saddle does not fail in a dramatic way resulting in an explosive water leak as happened in the case of the benchmark saddle. Second, the PowerSeal saddle has at least a 60% greater force capacity than that of the benchmark saddle. Third, the PowerSeal saddle has at least a 40% greater displacement capacity than that of the benchmark saddle. Fourth, the PowerSeal saddle with the original straps has similar displacement capacities but 47% greater force capacity than that of the one with the low-capacity straps.

According to the test results of fiber-optic sensors, the following was concluded. First, the fiber-optic result was validated by the strain gage data. Second, the PowerSeal saddle and the benchmark saddle would lead to similar strains on the pipeline. Third, the PowerSeal saddle with smaller torques tends to cause larger strains on the pipeline in terms of the magnitude. Fourth, the PowerSeal saddle with the low-capacity straps would result in smaller strains on the pipeline compared to the one with the original straps.

The experimental results were then compared to the finite element model. The strain distribution match well between the experiments and the simulation, indicating that the proposed FEM with the spring model can predict the behavior of this saddle test. Besides, the FEM shows the weakest area are the strap and the area between bolts and strap. The proposed model can be used in future parametric studies and as a reference for the future saddle design.

8 References

1. https://www.powerseal.com/psfiles/Models/3450AS_Technical_2020.pdf.
2. <https://www.3ds.com/support/hardware-and-software/simulia-system-information/abaqus-2020/>
3. https://www.engineersedge.com/coeffients_of_friction.htm

Appendix A: Specifications of PowerSeal saddle

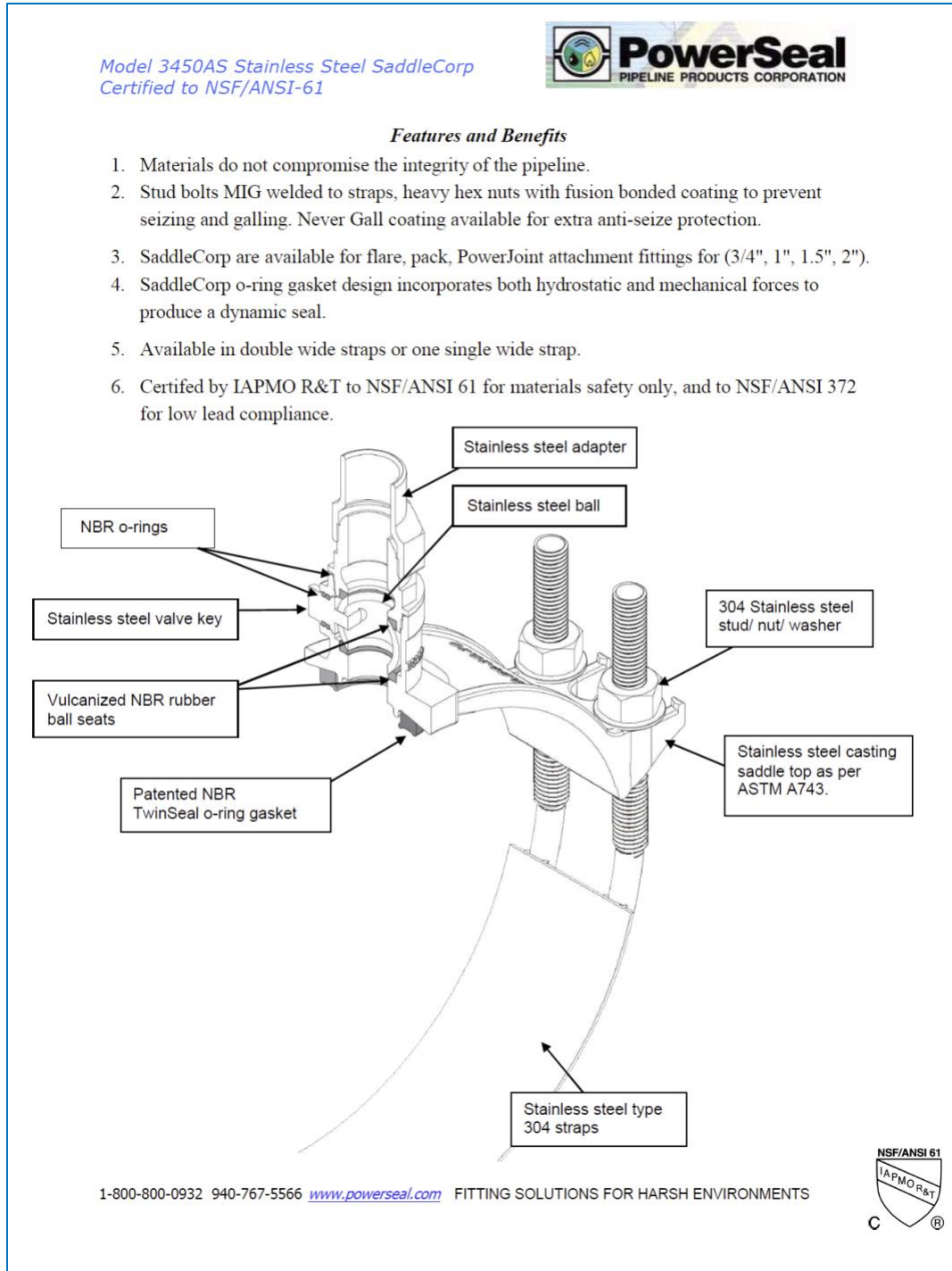


Figure A-1. Specifications of A 3450AS: page 1 (provided by PowerSeal).

Model 3450AS Stainless Steel SaddleCorp
 Certified to NSF/ANSI-61



Scope

The intent of the specification is to receive 3” diameter and up all cast body stainless steel SaddleCorp. The SaddleCorp furnished shall be equivalent to Model 3450AS as manufactured by PowerSeal Pipeline Products Corporation.

Design and Material Specification

The stainless steel SaddleCorp shall meet or exceed all material specifications as listed below:

1. SaddleCorp should incorporate both saddle and corp stop in one single cast piece, and shall be stainless steel as per ASTM A743.
2. The saddle body shall have an o-ring gasket permanently attached to the casting at the factory. The TwinSeal o-ring gasket along with all seals shall be made from NBR, they shall be free from porous areas, foreign material, and visible defects, all made from 100% new rubber. NBR can resist temperatures between -25 to +248°F.
3. The MIG welded strap shall be constructed of stainless steel type 304 and shall include weld attached 5/8” stainless steel 304 stud bolts. All welds shall be passivated to return their inherent corrosive resistance.
4. Adhesive will be used on adapters to prevent disassembly during installation.
5. There shall be no paper or plastic adhesive labels attached to the saddle, any information appearing on the saddle shall be ink stenciled.
6. SaddleCorp is NSF/ANSI 61 certified where applicable.

Material Specification

Part Name	Material	Mat. specs
SaddleCorp Body	Stainless Steel 18-8	ASTM A743
Strap	Stainless Steel Type 304	ASTM A240
Nuts & washers	Stainless Steel Type 304	ASTM A193
Corp gaskets	NBR	ASTM D2000
O-ring gasket	NBR	ASTM D2000
Parts (ball, adapter, key)	Stainless Steel 18-8	ASTM A743

1-800-800-0932 940-767-5566 www.powerseal.com FITTING SOLUTIONS FOR HARSH ENVIRONMENTS



Figure A-2. Specifications of A 3450AS: page 2 (provided by PowerSeal).

Model 3450AS Stainless Steel SaddleCorp
 Certified to NSF/ANSI-61



Model 3450AS



Flare

PowerJoint - CTS

Pack joint - IPS/CTS

Pipe Size		letter code	Pipe OD Range		Strap width
in.	mm.		in.	mm.	in.
3	80	B	3.45 - 4.05	88 - 103	1.5" each strap or 3" single wide strap small outlet 4" single wide strap big outlet
4	100	A	4.00 - 4.50	102 - 114	
		B	4.74 - 5.63	120 - 143	
6	150	C	4.74 - 5.14	120 - 131	
		A	6.00 - 6.63	152 - 168	
		B	6.84 - 7.64	174 - 194	
8	200	C	6.63 - 6.90	168 - 175	
		A	8.00 - 8.63	203 - 219	
		B	8.54 - 10.10	216 - 257	
10	250	C	8.63 - 9.05	219 - 229	
		A	10.00 - 11.10	254 - 282	
12	300	B	10.64 - 12.12	270 - 308	
		A	12.00 - 13.20	305 - 335	
		B	12.62 - 14.32	321 - 364	

1-800-800-0932 940-767-5566 www.powerseal.com FITTING SOLUTIONS FOR HARSH ENVIRONMENTS



Figure A-3. Specifications of A 3450AS: page 3 (provided by PowerSeal).

Appendix B: Photos of Tested Specimens



Figure B-1. Failure mode of benchmark saddle



Figure B-3. PowerSeal saddle with correct straps: after a test (typical)



Figure B-4. Side view of PowerSeal saddle: at completion of a test (typical)

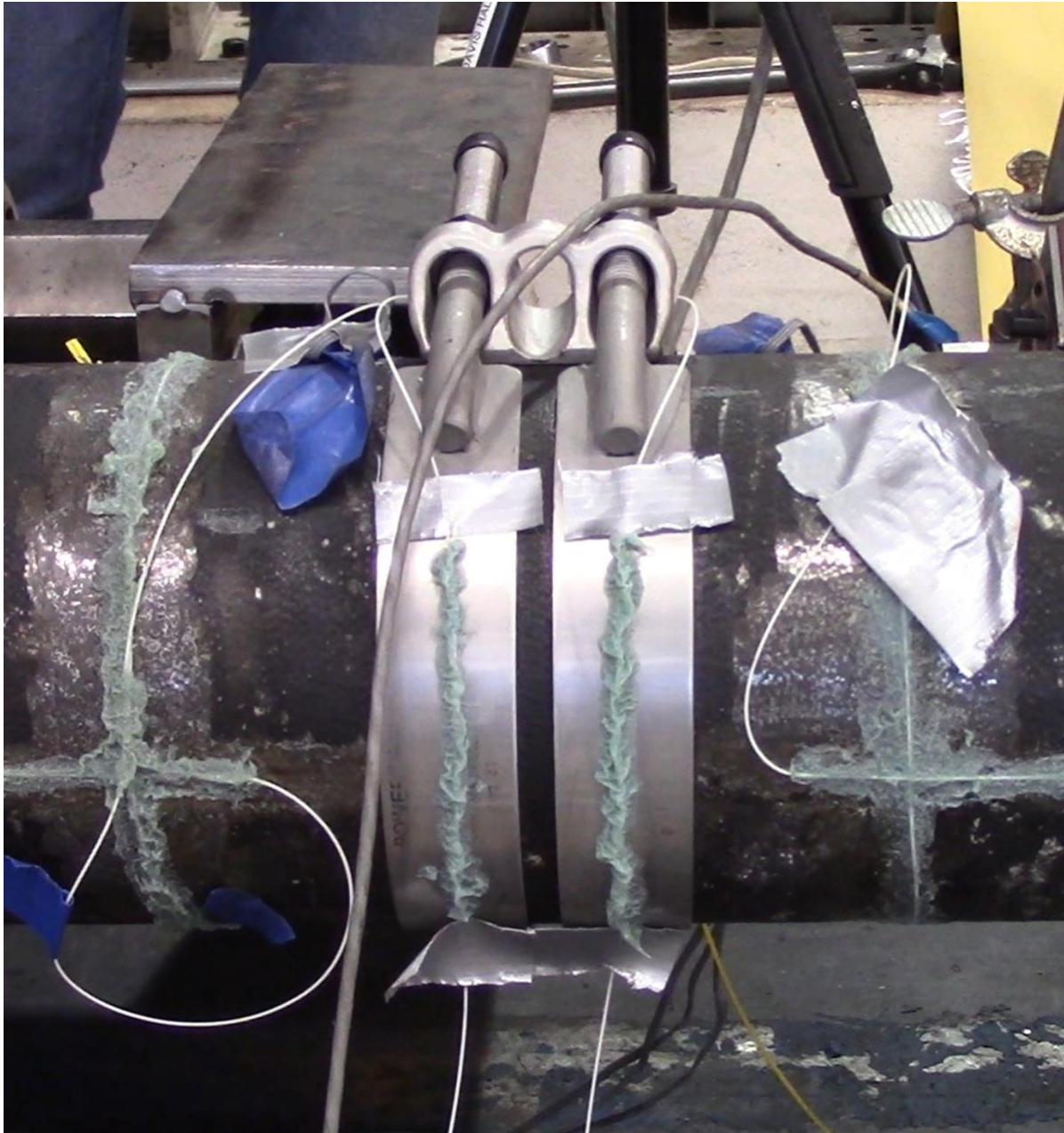


Figure B-5. PowerSeal saddle with correct straps: during a test (typical)

Appendix C: Distributed Fiber Optic Sensing

Using the physical properties of light, fiber-optic sensing can detect changes in temperature, strain, and other parameters when light travels along a fiber, which uses fiber-optic cables as sensors and can measure over long distances at 100 to 1000s of points on a single cable or multiplexed cables depending on the technology used. Compared to the other sensing technologies, fiber-optic sensing has distinct advantages such as small size, light weight, and strong resistance to corrosion and water.

LUNA Interrogator



Figure C-1. LUNA ODiSI 6000 Series optical distributed sensor interrogator

LUNA ODiSI 6104 is an optical distributed sensor interrogator, which can provide thousands of strain or temperature measurements per meter of a single high-definition fiber sensor. High-Definition (HD) Sensors - Strain & Temperature (HD-SC) temperature sensors utilize an advanced interrogation mode of the ODiSI to increase the accuracy of measurements when the sensors are subjected to strain, such as in embedded and surface-mount installations. It can achieve sensor gage pitch (the distance between two measurement points) as small as 0.65 mm, the sensor length up to 100 m, and measurement rate up to 250 Hz. More details about the LUNA interrogator can be found <https://lunainc.com/sites/default/files/assets/files/data-sheet/Luna%20ODiSI%206000%20Data%20Sheet.pdf>.

Fiber-optic Cable

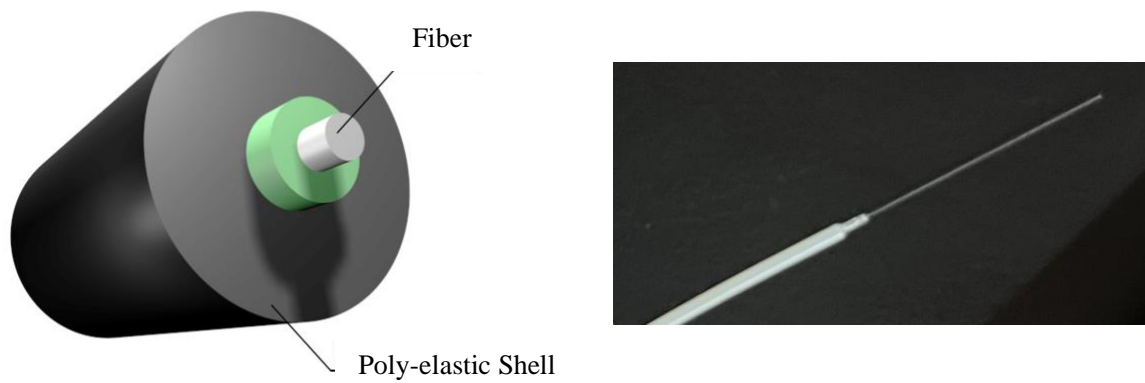
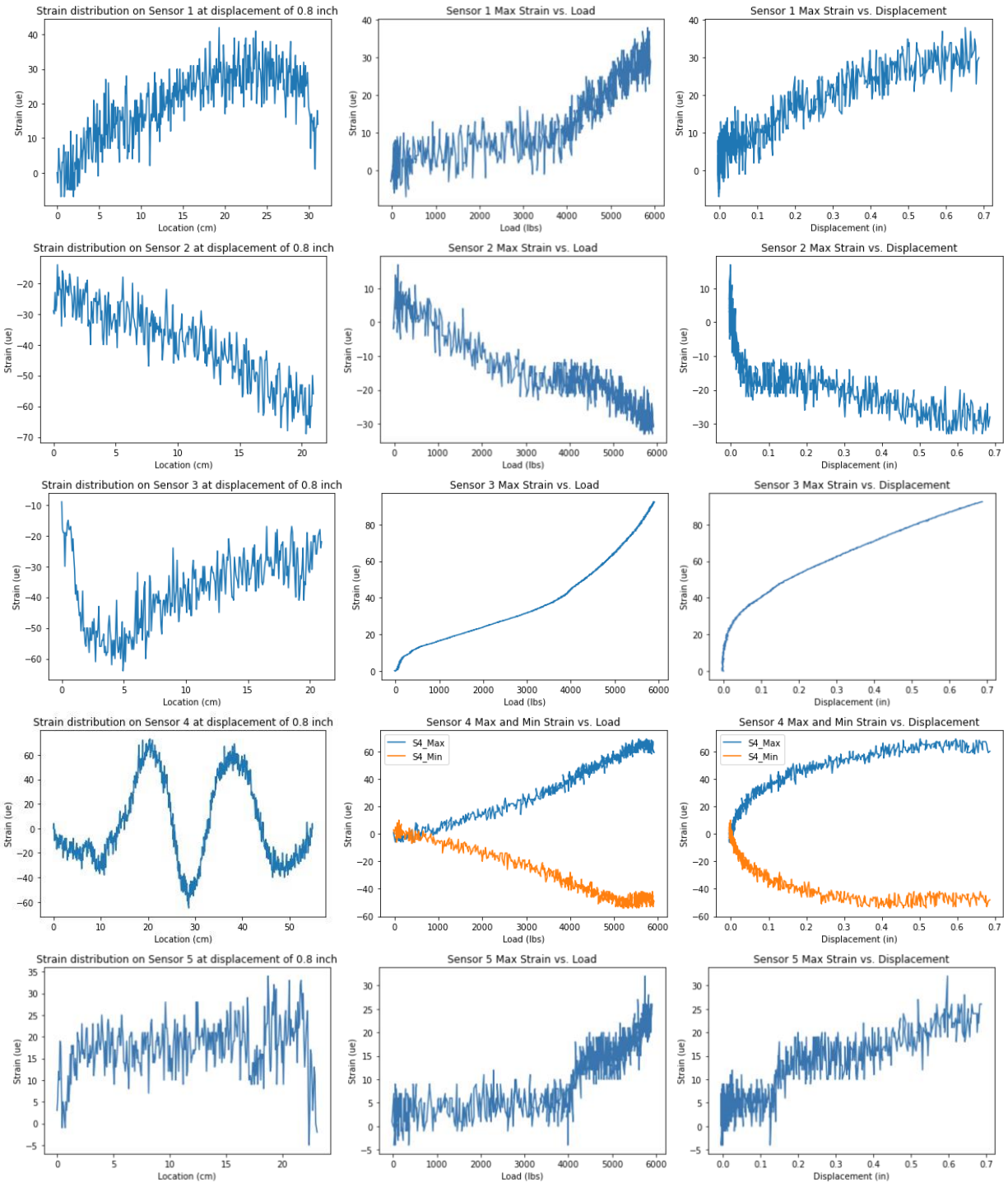


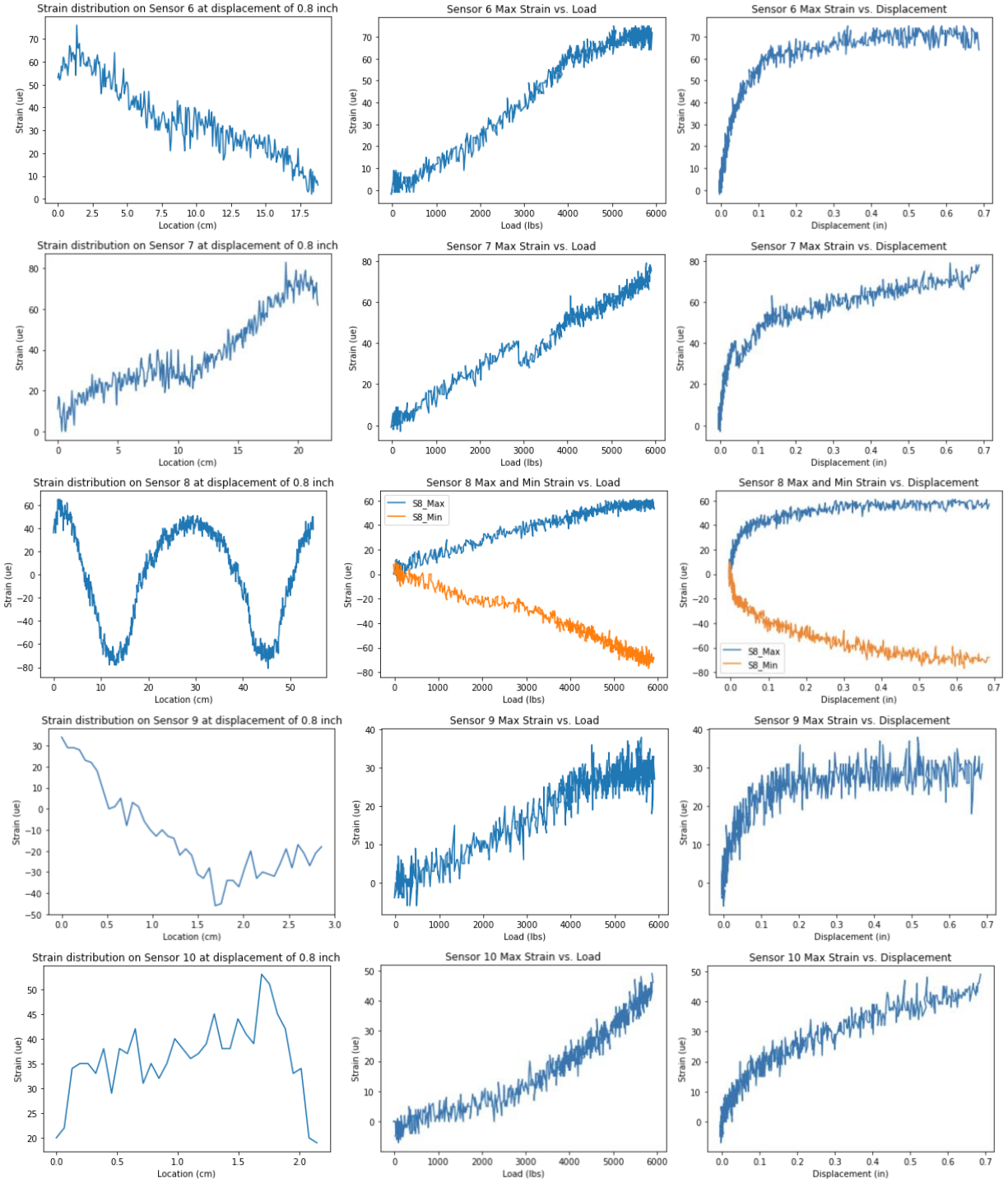
Figure C-2. NanZee NZS-DSS-C07 cable

NanZee NZS-DSS-C07 fiber-optic cable has a diameter of 0.9 mm, where the fiber is coated by a poly-elastic shell, which not only improves the strength and surface friction of the cable, but also reduces the overall rigidity and make it easier to be attached on the surface of the structure.

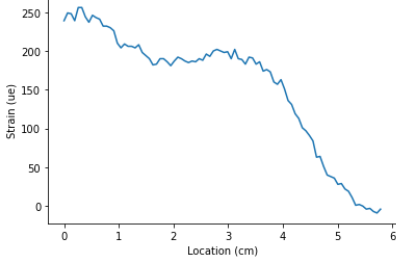
Appendix D: Test Results of Fiber-optic Sensors

Test Results for Benchmark1

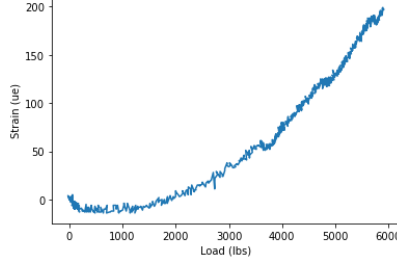




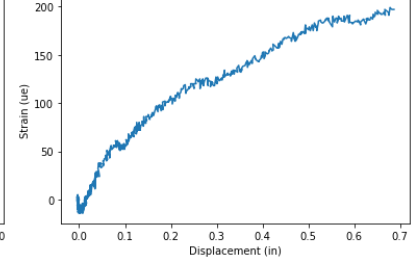
Strain distribution on Sensor 11 at displacement of 0.8 inch



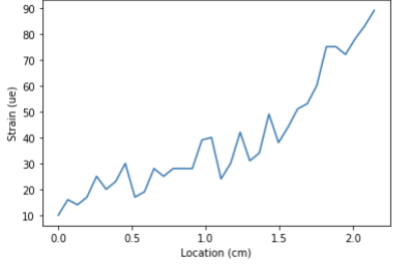
Sensor 11 Max Strain vs. Load



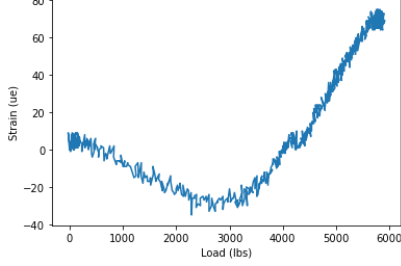
Sensor 11 Max Strain vs. Displacement



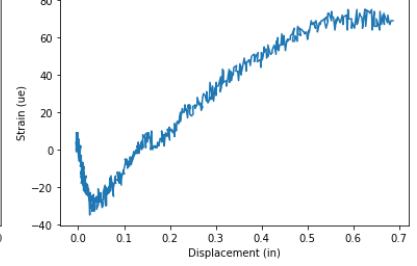
Strain distribution on Sensor 12 at displacement of 0.8 inch



Sensor 12 Max Strain vs. Load

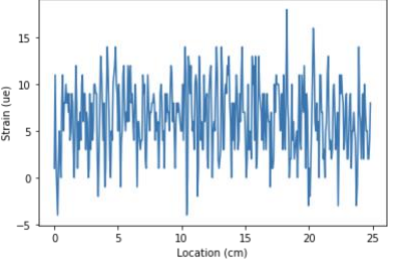


Sensor 12 Max Strain vs. Displacement

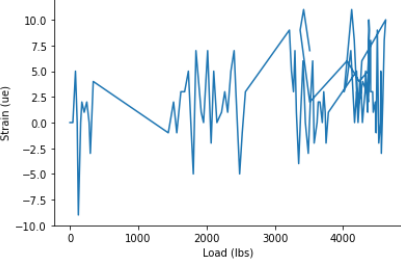


Test Results for Benchmark3

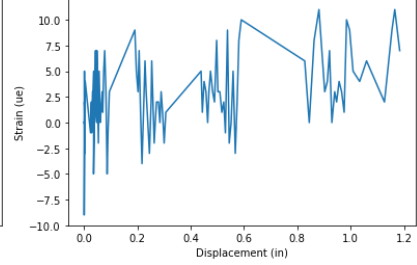
Strain distribution on Sensor 1 at displacement of 0.8 inch



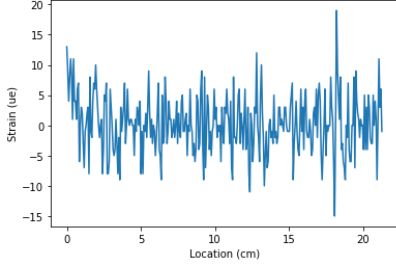
Sensor 1 Max Strain vs. Load



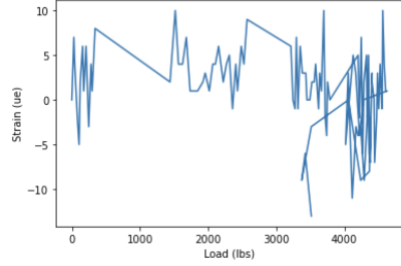
Sensor 1 Max Strain vs. Displacement



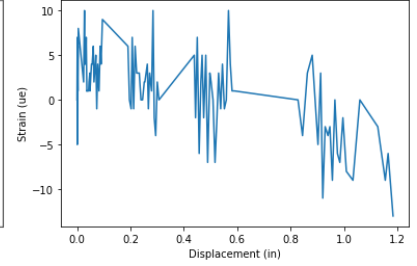
Strain distribution on Sensor 2 at displacement of 0.8 inch



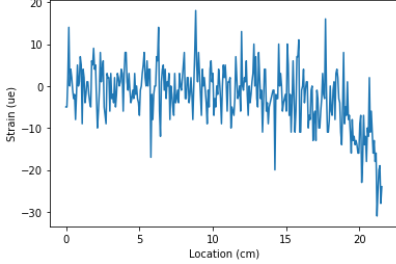
Sensor 2 Max Strain vs. Load



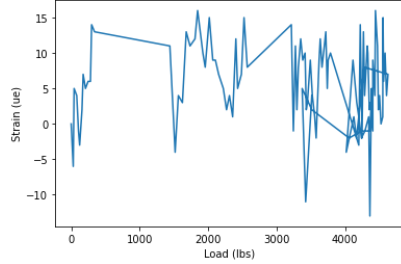
Sensor 2 Max Strain vs. Displacement



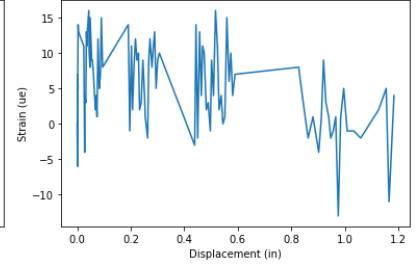
Strain distribution on Sensor 3 at displacement of 0.8 inch

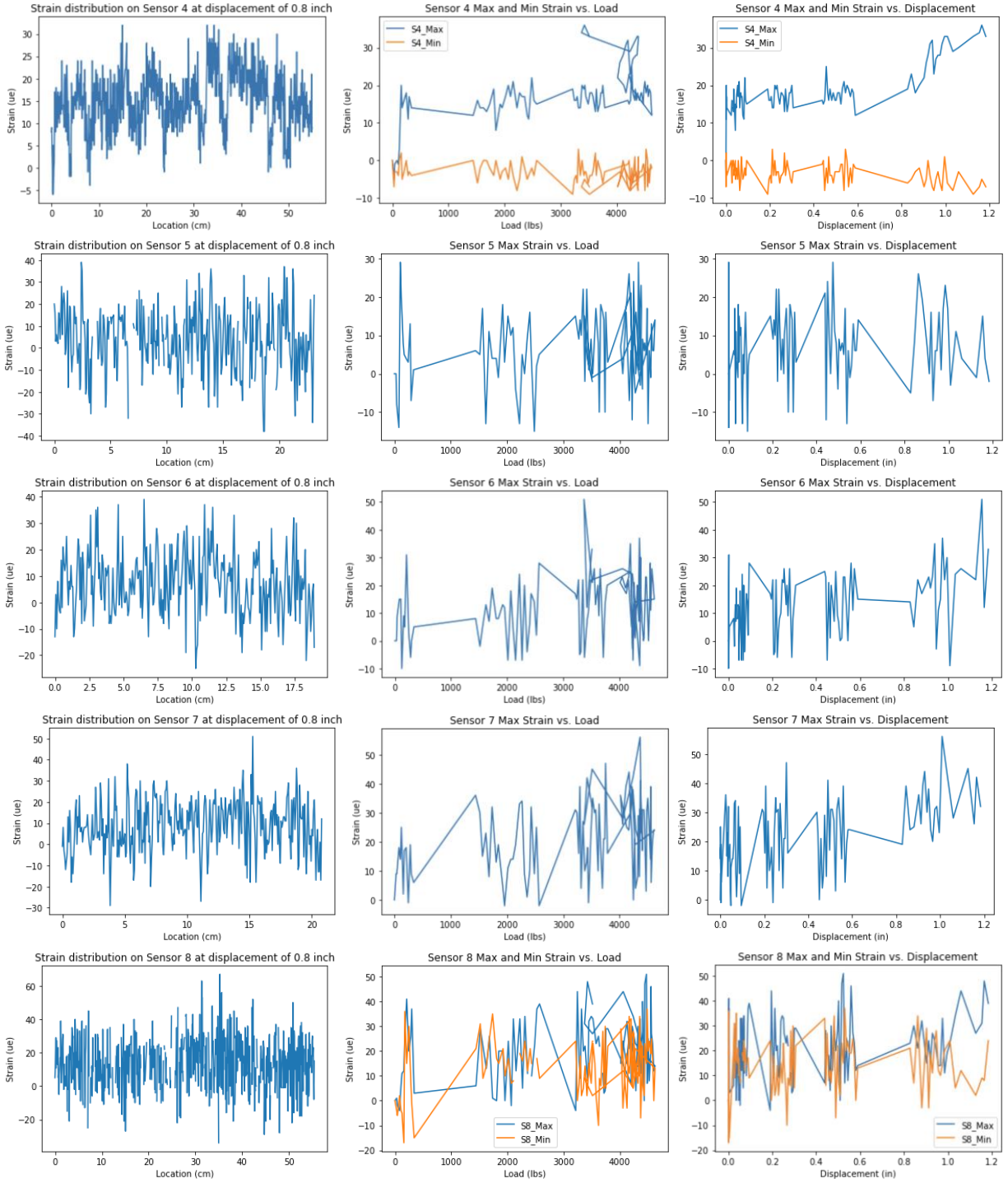


Sensor 3 Max Strain vs. Load



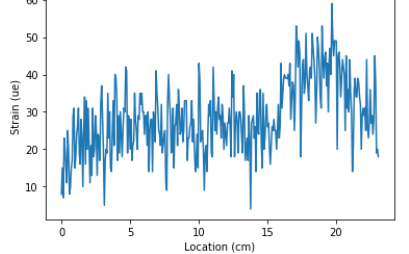
Sensor 3 Max Strain vs. Displacement



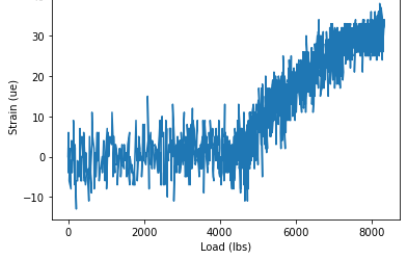


Test Results for PS1 (Sensor 1-4 had no data due to the channel connection issue)

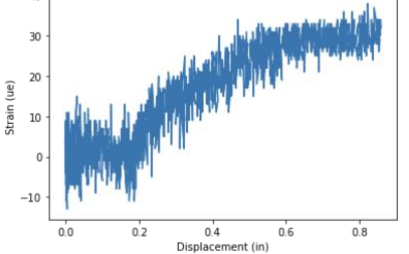
Strain distribution on Sensor 5 at displacement of 0.8 inch



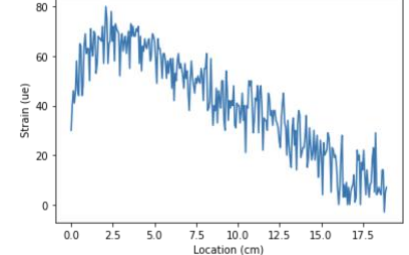
Sensor 5 Max Strain vs. Load



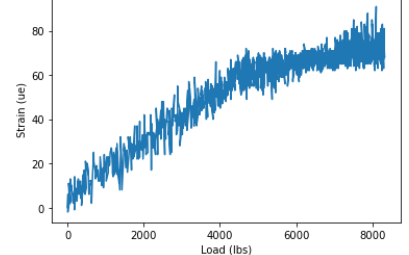
Sensor 5 Max Strain vs. Displacement



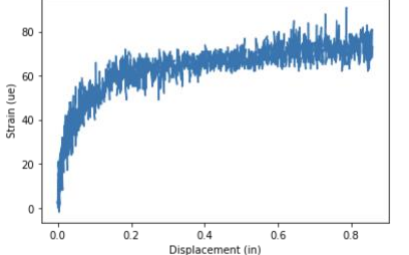
Strain distribution on Sensor 6 at displacement of 0.8 inch



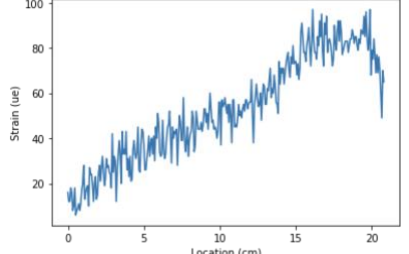
Sensor 6 Max Strain vs. Load



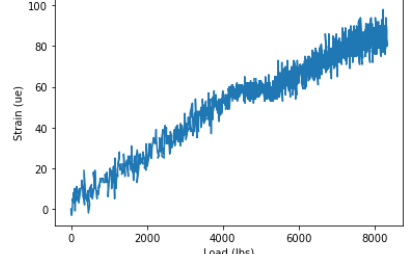
Sensor 6 Max Strain vs. Displacement



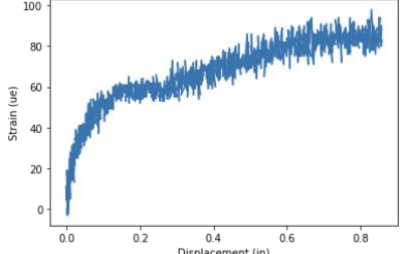
Strain distribution on Sensor 7 at displacement of 0.8 inch



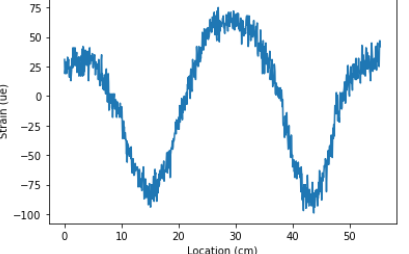
Sensor 7 Max Strain vs. Load



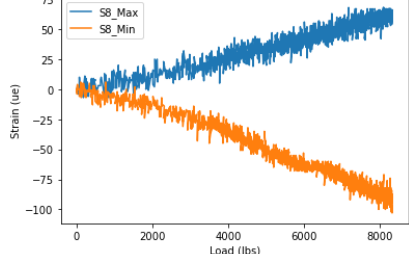
Sensor 7 Max Strain vs. Displacement



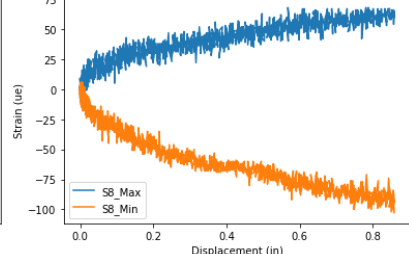
Strain distribution on Sensor 8 at displacement of 0.8 inch



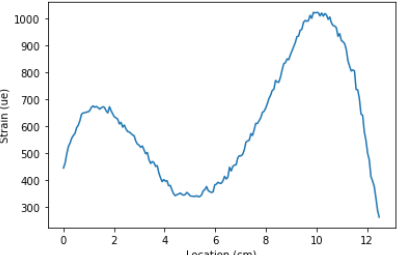
Sensor 8 Max and Min Strain vs. Load



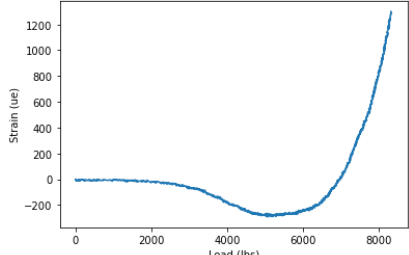
Sensor 8 Max and Min Strain vs. Displacement



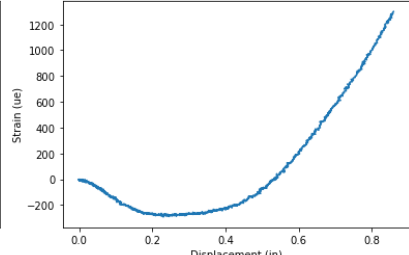
Strain distribution on Sensor 9 at displacement of 0.8 inch



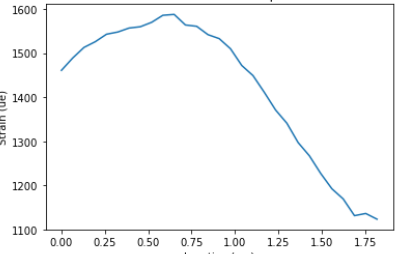
Sensor 9 Max Strain vs. Load



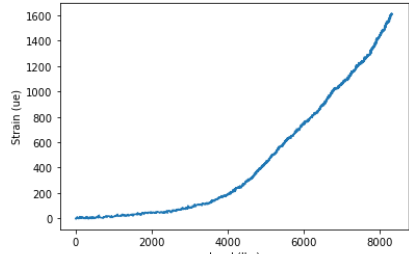
Sensor 9 Max Strain vs. Displacement



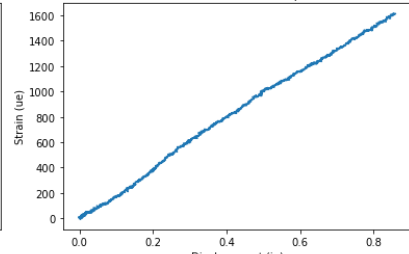
Strain distribution on Sensor 10 at displacement of 0.8 inch

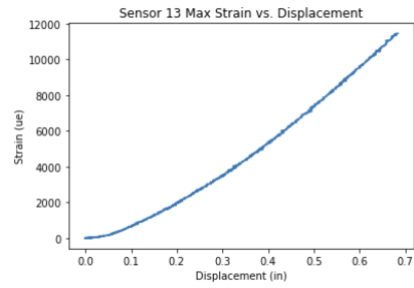
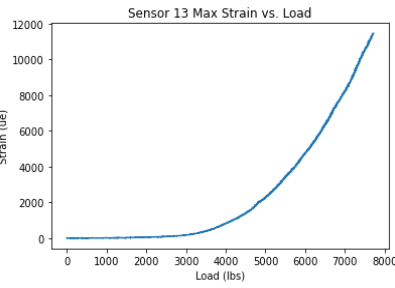
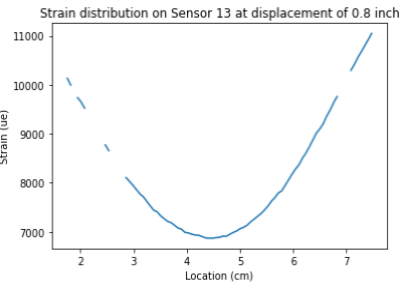
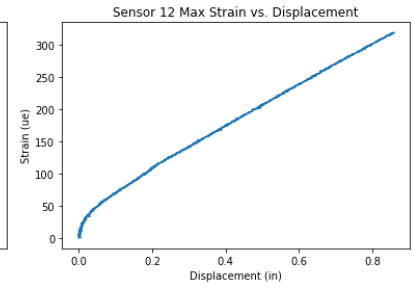
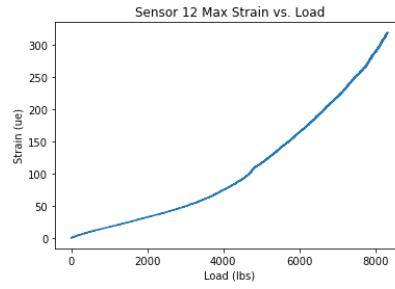
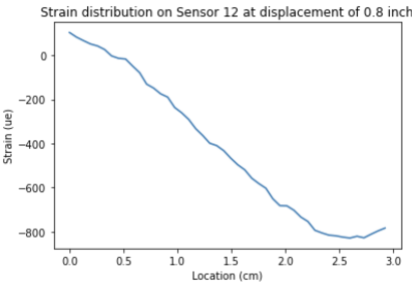
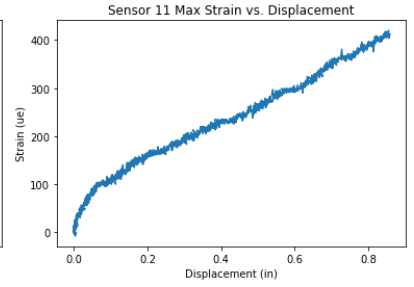
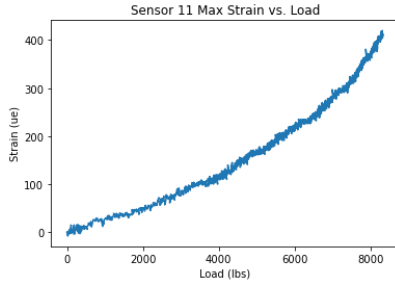
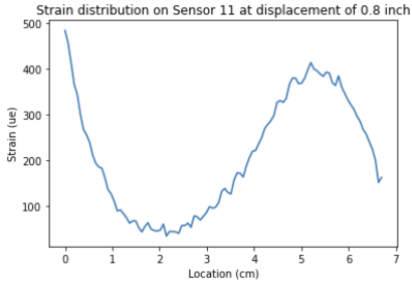


Sensor 10 Max Strain vs. Load

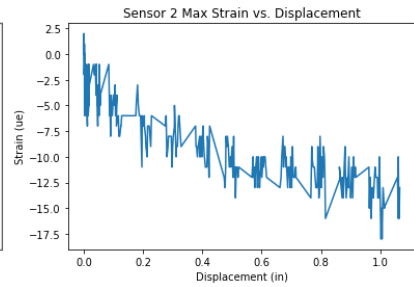
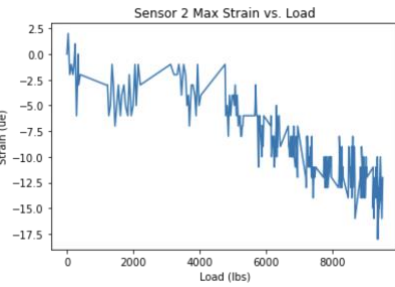
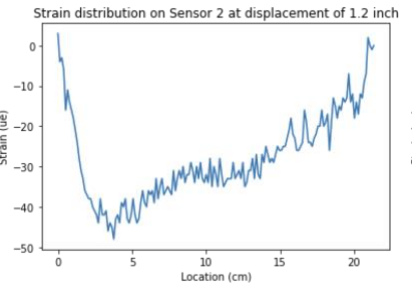
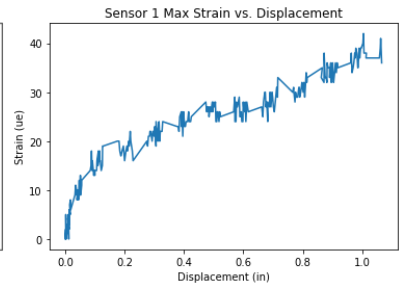
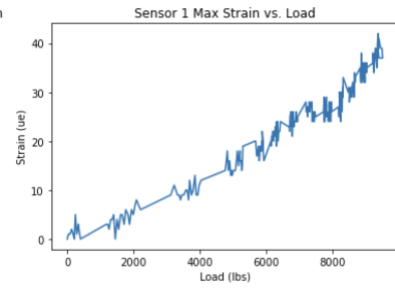
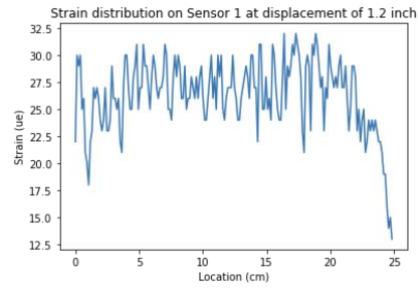


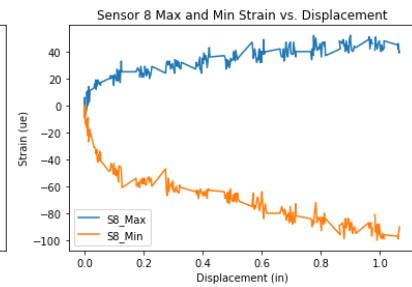
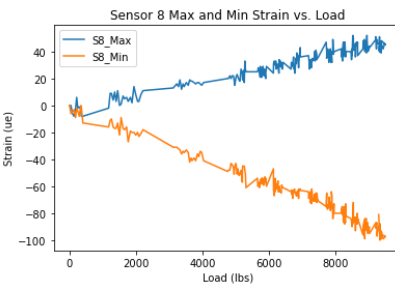
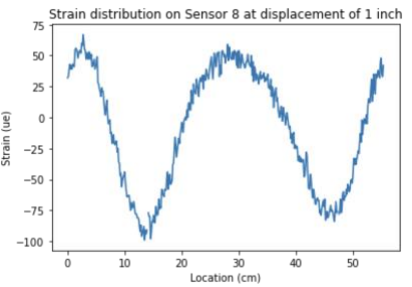
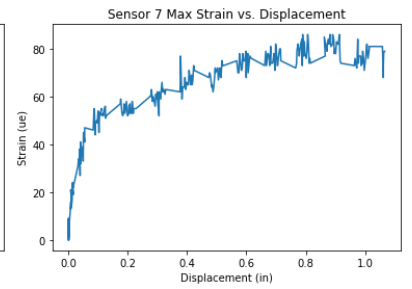
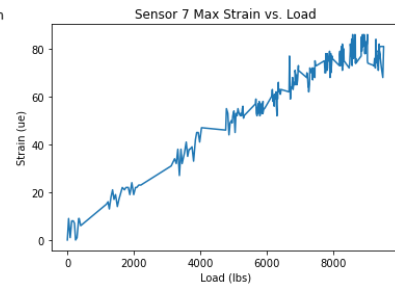
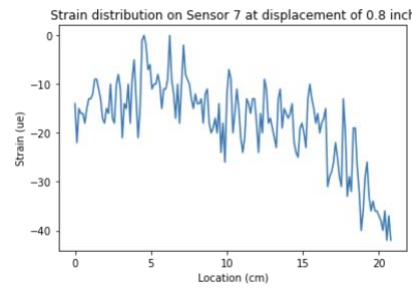
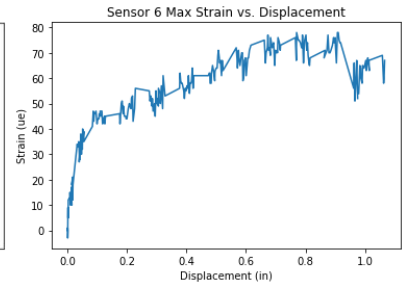
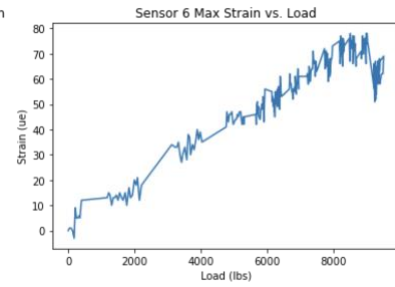
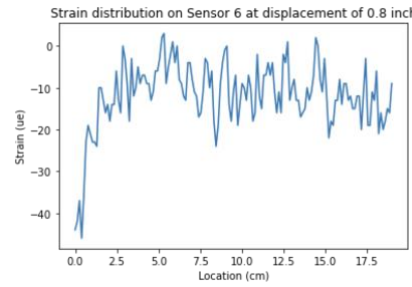
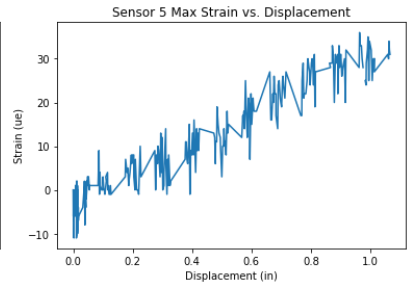
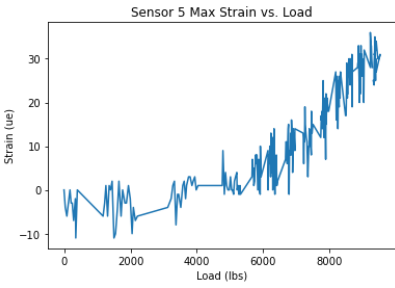
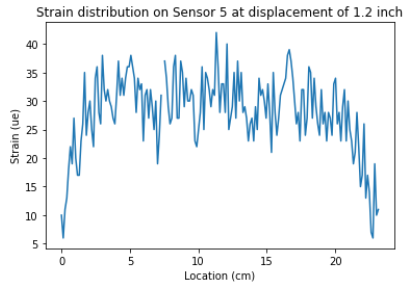
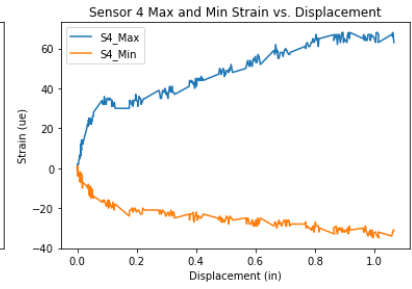
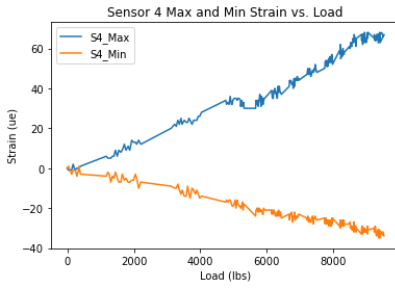
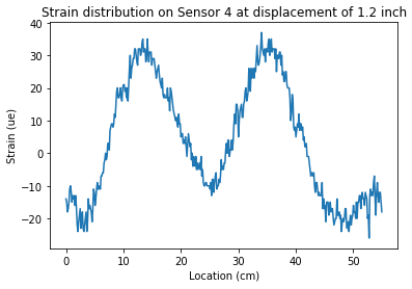
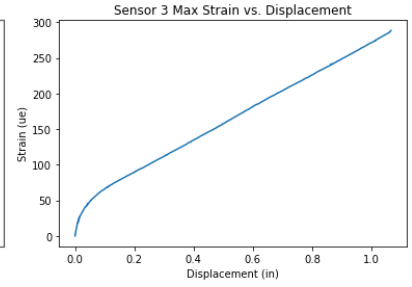
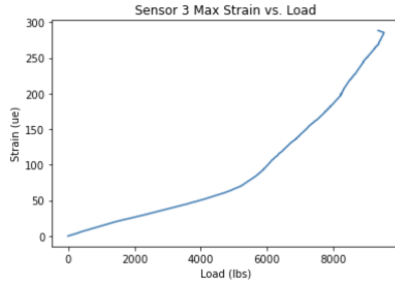
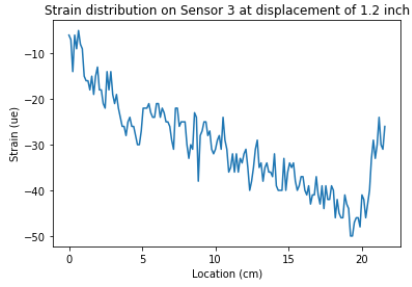
Sensor 10 Max Strain vs. Displacement

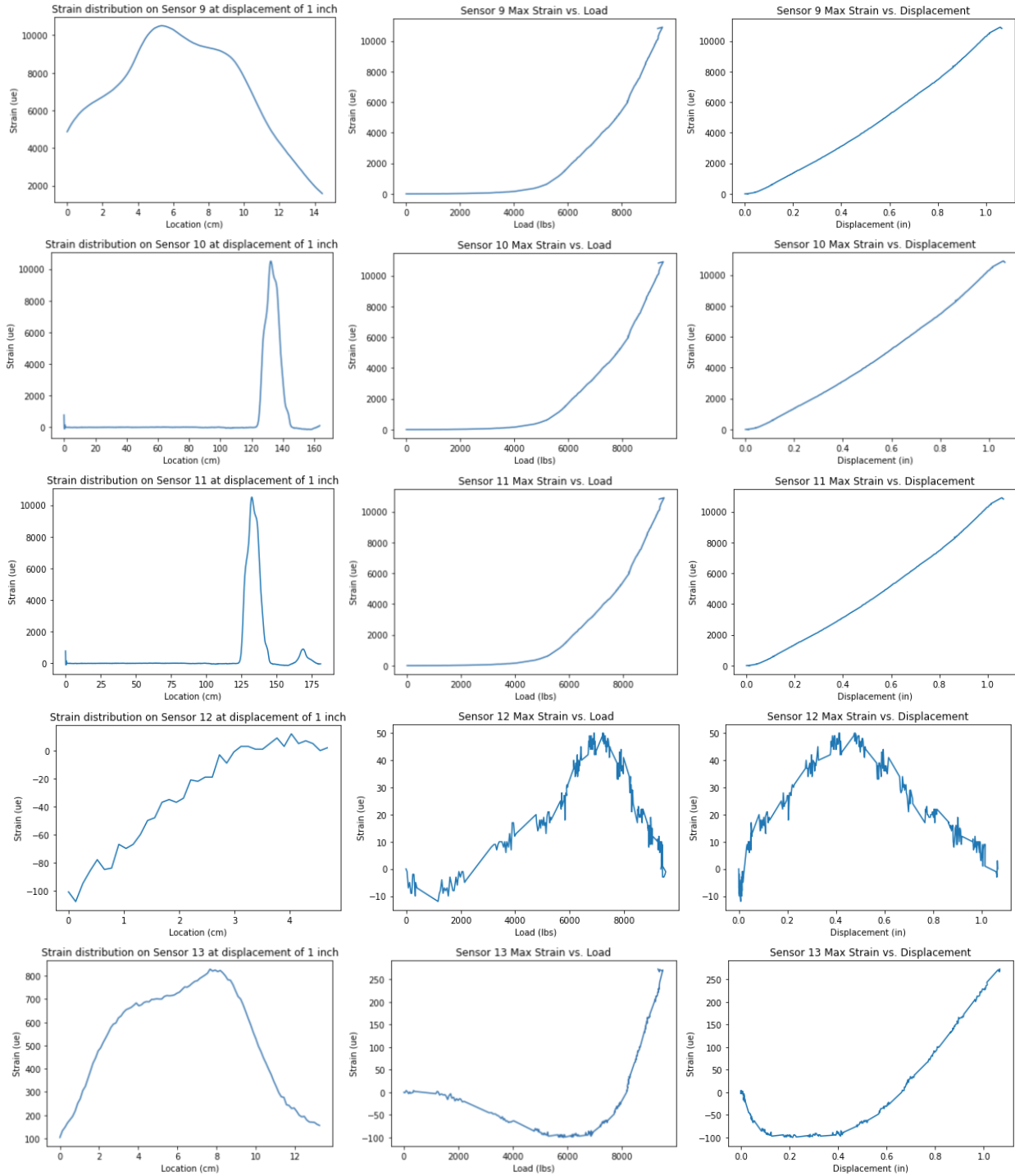




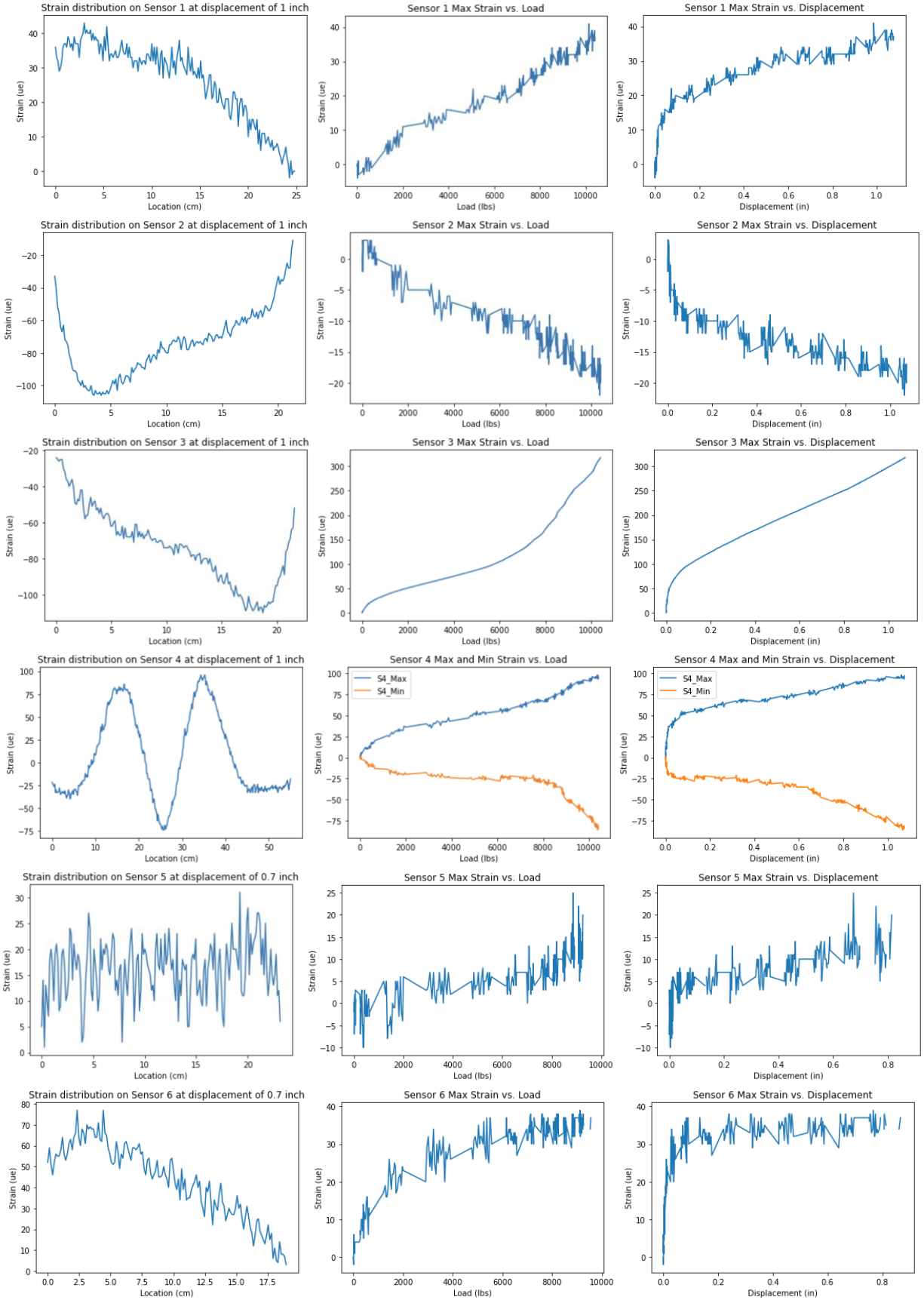
Test Results for PS2

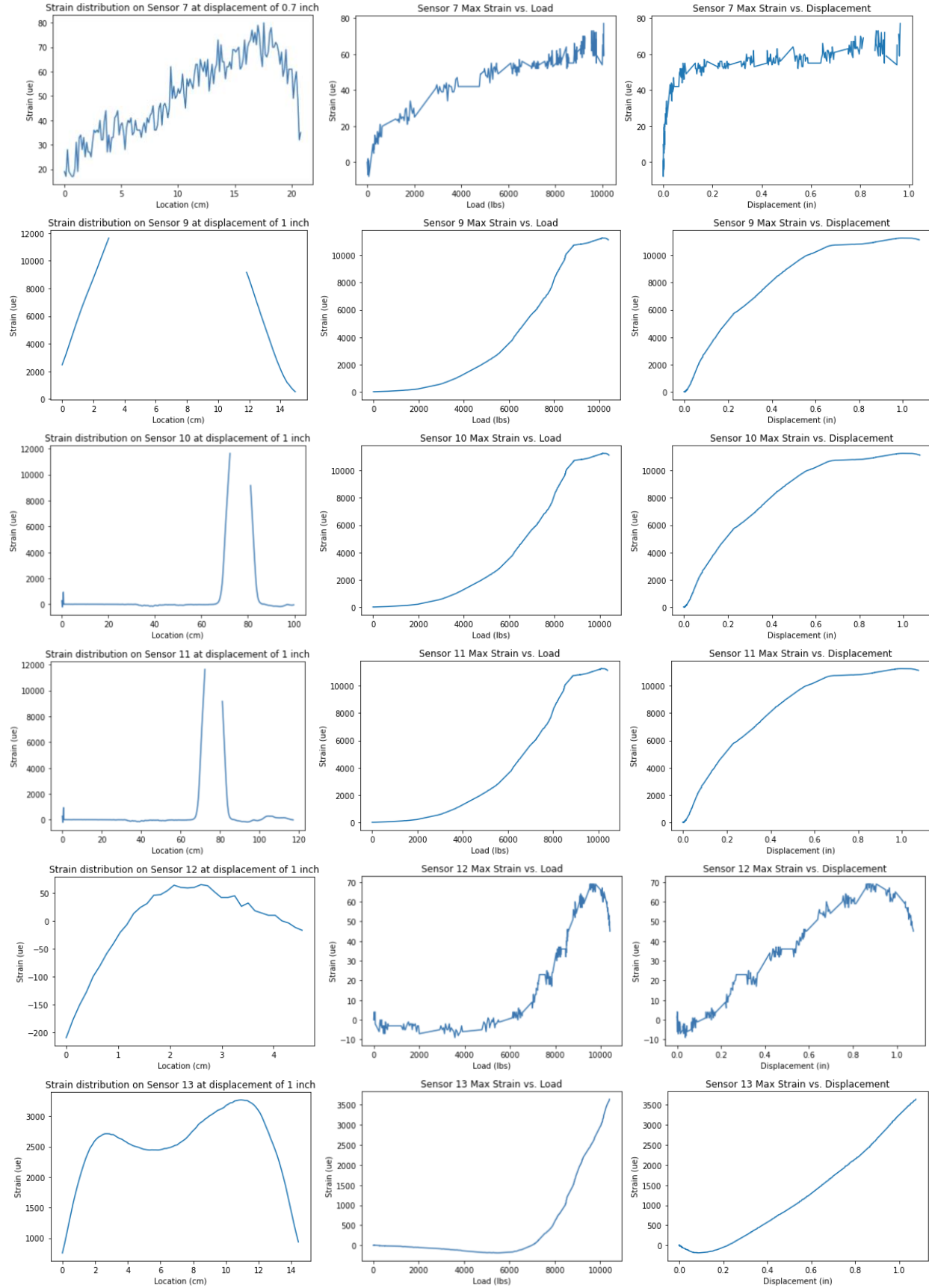




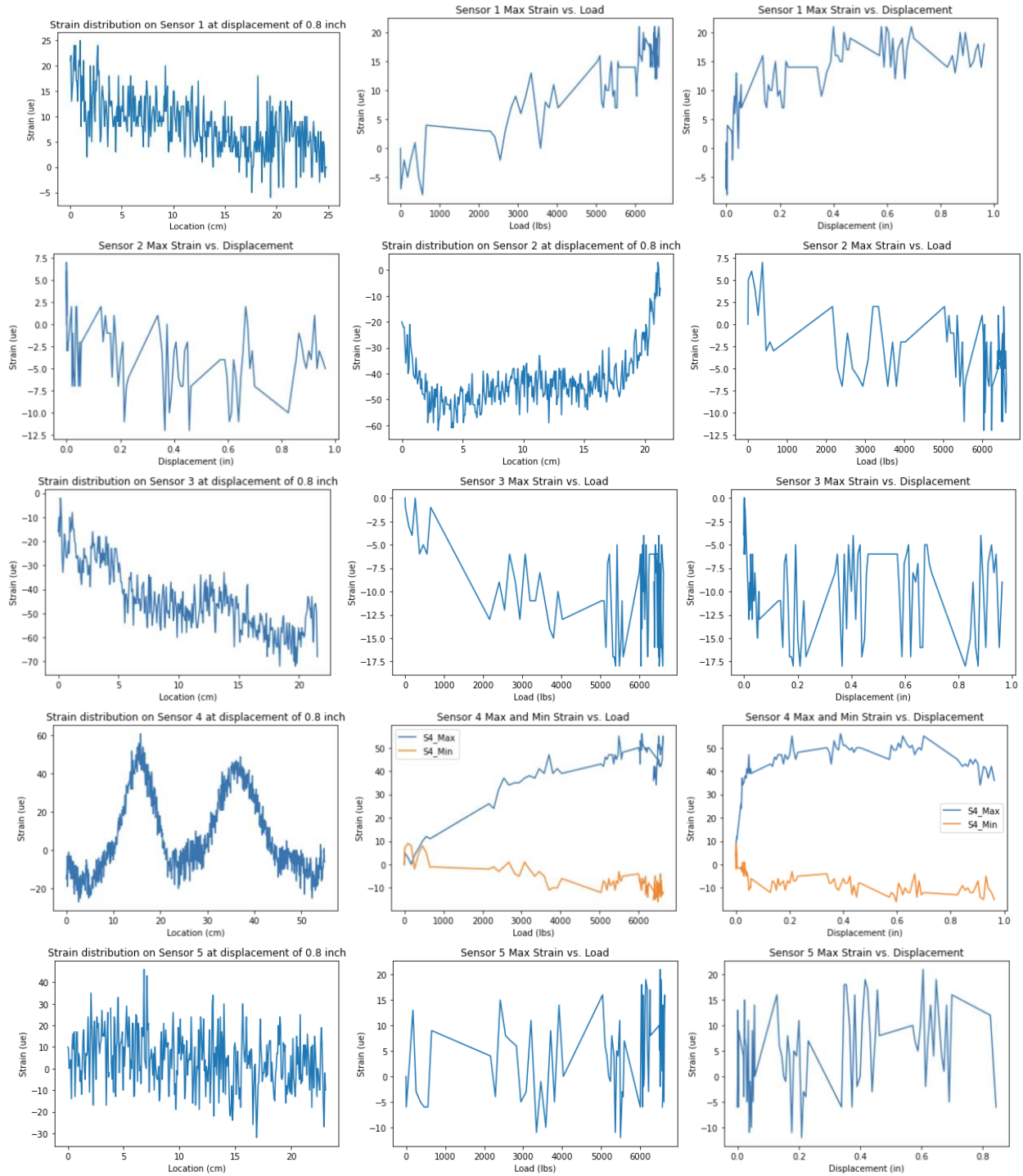


Test Results for PS3 (Sensor 9 is not included due to the weak signals)

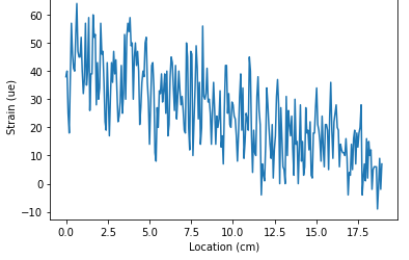




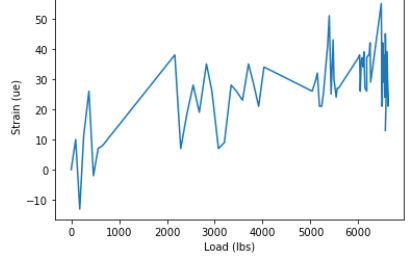
Test Results for PS2-NewStraps



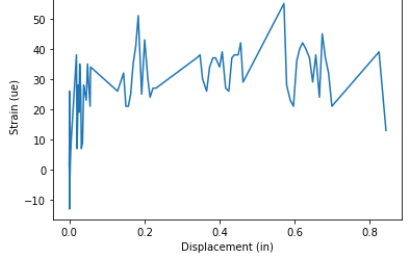
Strain distribution on Sensor 6 at displacement of 0.8 inch



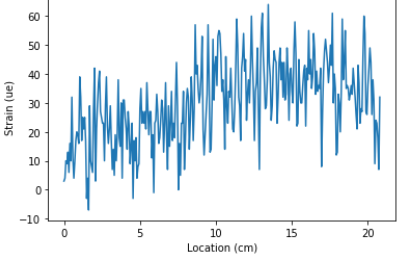
Sensor 6 Max Strain vs. Load



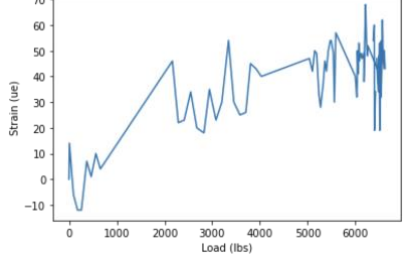
Sensor 6 Max Strain vs. Displacement



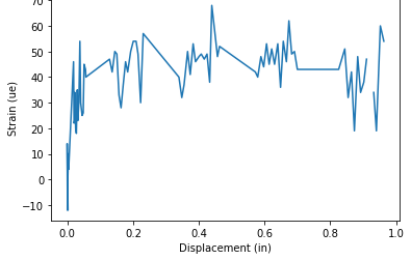
Strain distribution on Sensor 7 at displacement of 0.8 inch



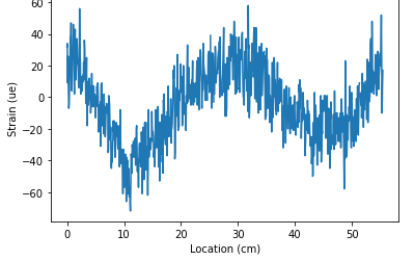
Sensor 7 Max Strain vs. Load



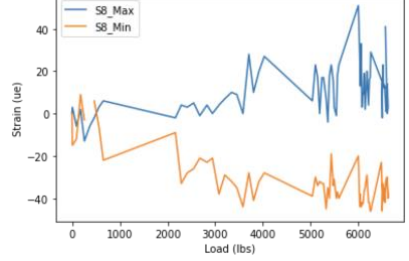
Sensor 7 Max Strain vs. Displacement



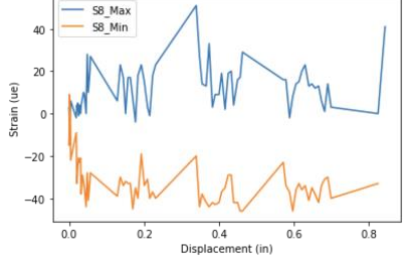
Strain distribution on Sensor 8 at displacement of 0.8 inch



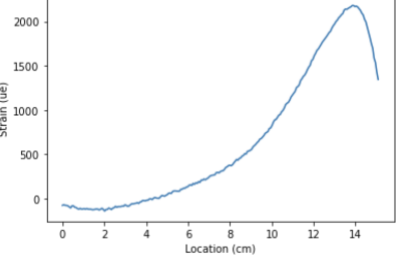
Sensor 8 Max and Min Strain vs. Load



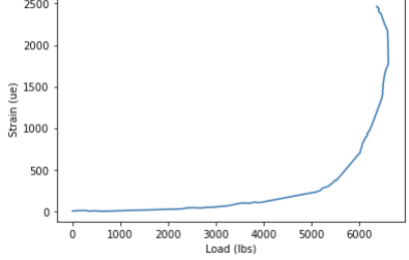
Sensor 8 Max and Min Strain vs. Displacement



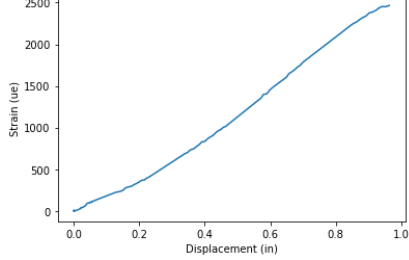
Strain distribution on Sensor 9 at displacement of 0.8 inch



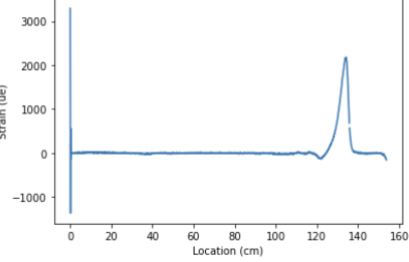
Sensor 9 Max Strain vs. Load



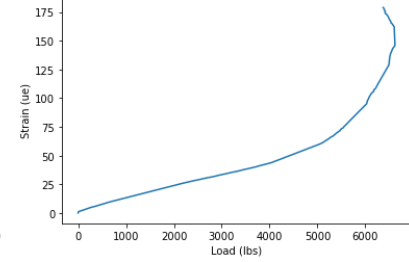
Sensor 9 Max Strain vs. Displacement



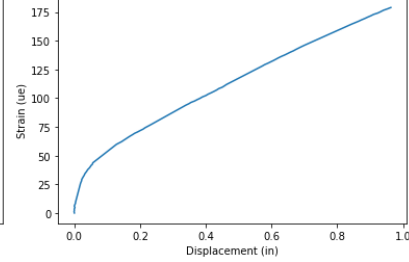
Strain distribution on Sensor 10 at displacement of 0.8 inch



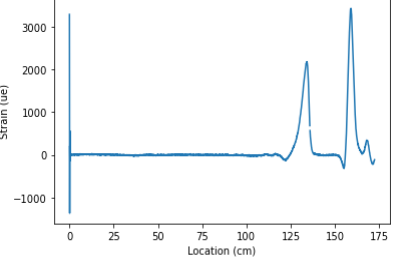
Sensor 10 Max Strain vs. Load



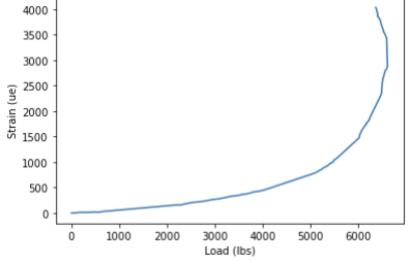
Sensor 10 Max Strain vs. Displacement



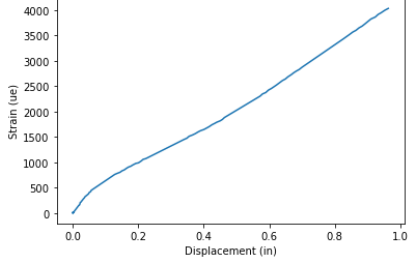
Strain distribution on Sensor 11 at displacement of 0.8 inch

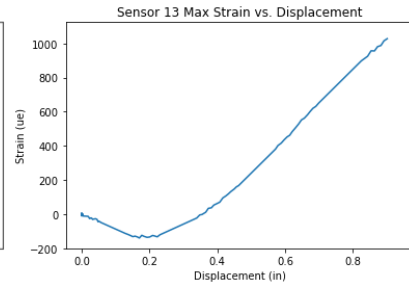
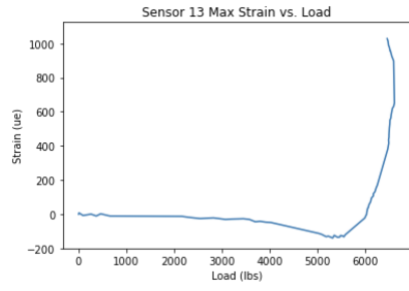
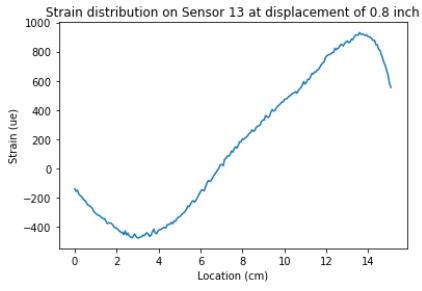
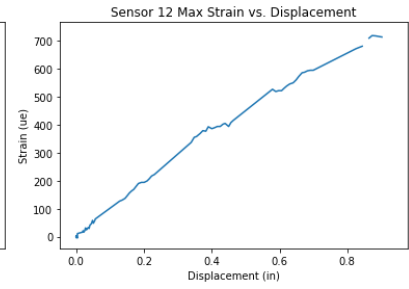
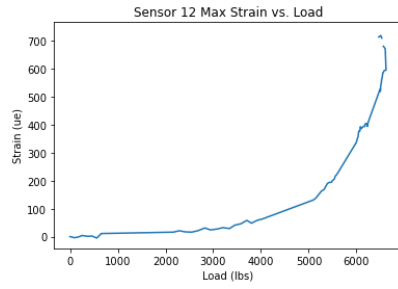
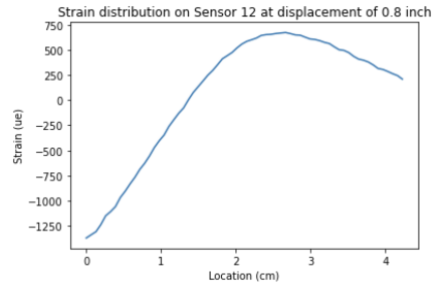


Sensor 11 Max Strain vs. Load



Sensor 11 Max Strain vs. Displacement





Appendix E: Finite Element Results

The comparison of the FEM results and FO data are presented below, where Sensor 10, Sensor 11, and Sensor 12 are not presented due to the uncertainty of the specific locations.

